Nuclear-Magnetic-Resonance Studies of Critical Phenomena in MnF_2. I. Time-Average Properties*

PETER HELLER
Physics Department, Brandeis University, Waltham, Massachusetts
(Received 26 January 1966)

A detailed experimental study is made of the F^{19} nuclear resonance in the antiferromagnet MnF_2 near its paramagnetic-antiferromagnetic critical point $T_N=67.34°K$. The dependence of the time-averaged sublattice magnetizations on temperature and external magnetic field is deduced from the behavior of the NMR frequencies. In zero external field the reduced sublattice magnetization is given by the cube-root law $M_0(T)/M_0(0)=1.20(1-T/T_N)^{0.333\pm0.003}$. It was possible to make measurements up to within about 5 mdeg of T_N and so demonstrate that this law holds with remarkable precision over the reduced temperature range $0.92<T/T_N<0.99993$. The corresponding range in reduced magnetization was from 0.50 to 0.05. The influence of an external field on the sublattices was studied in detail. In addition to field-proportional changes in the magnetizations, nonlinear effects occur which can be associated quantitatively with the observed downward shift in the Néel temperature produced by the field. A theoretical discussion of the magnetic critical behavior is made using the molecular-field approximation. It is found that the experimentally observed relation between the nonlinear effects of the applied field and the shift of the Néel point is a property of the molecular-field model near T_N. However, the observed shift is about three times the calculated shift. An accurate experimental determination of the effect of hydrostatic pressure on the Néel temperature is made. The result, $dT_N/dP=(3.03\pm0.03)\times10^{-4}$ °K/kg/cm², is used together with thermal-expansion data to estimate that the magnetic critical behavior of MnF_2 corrected to the case of fixed lattice parameters is described by $M_0(T)/M_0(0)=1.19(1-T/T_N)^{0.335\pm0.005}$.

1. INTRODUCTION AND SUMMARY

MAGNETIC systems provide situations in which accurate experimental studies of co-operative phenomena can be carried out. In particular the technique of nuclear magnetic resonance (NMR) yields very precise information of interest in the statistical mechanical theories. Well below the ordering temperature, i.e., the Curie or Néel point, such measurements make possible a detailed examination of the theory of spin waves and their interactions. In studying phase transitions however, the most interesting region is the immediate vicinity of the ordering temperature. This is a temperature which is closely analogous to the critical point for condensation in fluid systems. In this, the first of two papers, we begin a detailed account of experiments[1–3] carried out on the F^{19} nuclear resonance in the antiferromagnet MnF_2 near its Néel point $T_N=67.34°K$. These experiments provide a detailed and precise description of the critical phenomena associated with the magnetic transition.

Broadly speaking, two types of experimental information are obtained:

(i) The time-averaged sublattice magnetization M is determined as a function of temperature and external magnetic field. In particular it will be shown that in zero external field the relation

$$M \propto (T_N-T)^{1/3} \tag{1}$$

holds with remarkable accuracy just below T_N. This is strikingly similar to the behavior of the difference in densities between the coexisting liquid and vapor phases observed experimentally near fluid critical points.[4–6]

(ii) The behavior of the NMR linewidths show that large fluctuations in the magnetization take place near T_N. This effect is closely related to the phenomenon of critical opalescence occurring near a liquid-gas critical point. The linewidth results, together with a theoretical discussion, will be presented in the second paper, hereafter referred to as II.

Bloembergen and Poulis[7] attempted to observe the F^{19} resonance in MnF_2. However, the linewidth was too large for the equipment then available and the first successful application of NMR to the study of magnetic ordering was carried out by Poulis and Hardeman on the proton resonances in hydrated copper salts.[8] They showed for the first time that the time-average spin polarizations on each sublattice give rise to a nonzero NMR frequency in zero external field. They found that the magnetic-ordering process takes place more rapidly than is predicted on the molecular-field model. However, the proton resonance data did not provide an accurate account of $M(T)$ near T_N.

The F^{19} resonance in MnF_2 was first found by Shul-

* The experiments described here were performed at the Gordon McKay Laboratory, Harvard University, with the support of the U. S. Joint Services. The data analysis in parts I and II and the theory in part II were prepared at the Massachusetts Institute of Technology, Cambridge, Massachusetts, with the support of the Advanced Research Projects Agency, Contract No. SD-90. The material in Secs. 5 and 6 of part I was prepared at Brandeis University with the support of the U. S. Air Force Office of Scientific Research, Grant No. 871-65.

[1] P. Heller and G. B. Benedek, Phys. Rev. Letters **8**, 428 (1962).
[2] P. Heller and G. B. Benedek, in *Proceedings of the First International Conference on Paramagnetic Resonance*, edited by W. Low (Academic Press Inc., New York, 1963), Vol. II.
[3] P. Heller, thesis, Harvard University, 1963 (unpublished).
[4] E. A. Guggenheim, J. Chem. Phys. **13**, 253 (1945).
[5] M. A. Weinberger and W. G. Schneider, Can. J. Chem. **30**, 422 (1952).
[6] M. E. Fisher, J. Math. Phys. **5**, 944 (1964).
[7] N. Bloembergen and N. J. Poulis, Physica **16**, 915 (1950).
[8] N. J. Poulis and G. E. G. Hardeman, Physica **18**, 201 (1952).

man and Jaccarino.[9] They showed that a strong and largely isotropic hyperfine interaction existed between the manganese spins and the fluorine nuclei, the saturated sublattices at 0°K giving rise to a F^{19} NMR frequency

$$\nu_{00}=159.978 \text{ Mc/sec.} \quad (2)$$

In subsequent studies, Jaccarino and Walker[10] obtained the zero-field sublattice magnetization $M_0(T)$ from the zero-field NMR frequency $\nu_0(T)$, using the relation

$$M_0(T)/M_0(0)=\nu_0(T)/\nu_{00}. \quad (3)$$

Their measurements extended up to 55°K.

In their original work, Shulman and Jaccarino observed the line in the paramagnetic state $T>T_N$. They reported the disappearance of the line as the sample was cooled through the Néel point, their temperature control being insufficient to follow the line through the transition. Thus, prior to the present work, no precise measurements in magnetic systems had been made in the very important region near the critical point.

The measurements presented here required an experimental system permitting temperature measurement and control to within one millidegree for several hours, together with the detection of nuclear resonances of width up to 3 Mc/sec. The techniques developed for this purpose will be discussed in Sec. 2.

In some measurements close to T_N, an adequate signal-to-noise ratio could only be achieved by using an external field $\mathbf{H}_0$ to bring the F^{19} resonance frequency above $\approx$25 Mc/sec. Since we wished to study the behavior of MnF_2 in zero field, it was necessary to have a precise understanding of the effect of $\mathbf{H}_0$ on the resonances. Aside from the simple additive contribution of $\mathbf{H}_0$ to the field at the nucleus, the alteration in the NMR frequency occurring upon application of the field is due to its effect on the manganese spin sublattices. This effect is in part a field-proportional polarization described by a susceptibility. However, we will see that the field also has the effect of depressing the Néel temperature. In the present experiments this shift was slight, being less than 13 mdeg. Associated with this shift, however, nonlinear terms appear in the field dependence of the sublattice magnetizations and hence in that of the NMR frequencies. A phenomenological theory of these effects, which was verified experimentally, is presented in Sec. 3. Once these effects were understood, the shift in the Néel point could be taken very carefully into account. It was then possible to realize the full power of the NMR method of determining the zero-field behavior $M_0(T)$.

The experimental data are presented in Sec. 4. In Sec. 4A we present the results of a direct and accurate determination of the effect of hydrostatic pressure[11] on T_N. Such a measurement provides information on the dependence on the lattice parameters of the superexchange forces thought to be responsible for the antiferromagnetism. In addition to being interesting in itself, this information is important in estimating the effect of thermal expansion on the magnetic behavior.

In Sec. 4B we present direct measurements of the shift of the Néel point in an applied field. In measuring both the field and pressure dependences, changes in the Néel point were determined by utilizing the rapid fade-out of the NMR lines which takes place as T approaches T_N from above.

In Sec. 4C we present the results of very careful observations of the behavior of the resonances in an applied field. From these measurements, the temperature dependences of the sublattice susceptibilities were determined and found to be in agreement with bulk-susceptibility data.[12,13] More importantly, the nonlinear terms in the field dependence of the sublattice magnetizations were measured and found to agree with the predictions of the phenomenological theory given in Sec. 3, using the experimental results for the field dependence of T_N. We note here that bulk magnetization measurements could not reveal the presence of these nonlinear effects as they arise from equal and opposite changes in the magnetizations of the two sublattices.

The behavior of the zero-field NMR frequency $\nu_0(T)$ could then be determined with a precision corresponding to an uncertainty of a few millidegrees in the measured temperature. The data start at about 5 mdeg below T_N, at which point $\nu_0(T)$ is about 5% of its saturation value. The data are fitted to an expression[14] of the form

$$\nu_0(T)/\nu_{00}=D(1-T/T_N)^{\beta}, \quad (4)$$

a very precise fit being obtained for the reduced temperature range $0.92<T/T_N<0.99993$. This provides an insight into the extent of the "critical region." The value of β required for the fit is

$$\beta=0.333\pm0.003, \quad (5)$$

while

$$D=1.200\pm0.004 \quad \text{and} \quad T_N=67.336\text{°K}. \quad (6)$$

These results are presented in Sec. 4D.

The molecular-field theory of magnetism due originally to Weiss[15] has frequently been applied to antiferromagnetic phenomena[16–20] where it has provided many valuable insights. In Sec. 5 we apply the theory

[9] R. G. Shulman and V. Jaccarino, Phys. Rev. **108**, 1219 (1956); **107**, 1196 (1957).
[10] V. Jaccarino and L. R. Walker, J. Phys. Radium **20**, 341 (1959).
[11] G. B. Benedek and T. Kushida, Phys. Rev. **118**, 46 (1960).
[12] J. W. Stout and M. Griffel, J. Chem. Phys. **18**, 1455 (1950).
[13] H. Bizette and B. Tsai, Compt. Rend. **238**, 1575 (1954).
[14] J. W. Essam and M. E. Fisher, J. Chem. Phys. **38**, 802 (1963).
[15] P. Weiss, J. Phys. **6**, 667 (1907).
[16] L. Néel, J. Phys. Radium **3**, 160 (1932).
[17] F. Bitter, Phys. Rev. **54**, 79 (1937).
[18] J. H. Van Vleck, J. Chem. Phys. **9**, 85 (1941).
[19] C. G. B. Garrett, J. Chem. Phys. **19**, 1154 (1951).
[20] T. Nagamiya, K. Yosida, and R. Kubo, Advan. Phys. **4**, 2 (1955) (review article).

in interpreting the results of the present experiments. Some standard results will be reviewed and new results dealing with the nonlinear effects of the applied field on the sublattices will be derived. In the experiments it was found that the nonlinear behavior is governed by a "law of corresponding states" according to which the magnetizations of the sublattices depend on T_N through their dependence on the reduced temperature T/T_N. We shall show that this behavior is indeed a property of the molecular field model near T_N. However we will find that the observed Néel point depression is about 3 times larger than is predicted. The effect of an external field in quenching the antiferromagnetism is thus stronger in reality than in the molecular field model. A nice illustration of this result is provided by considering the effect of applying a field **H** at right angles to the antiferromagnetic axis. Experimentally it is found that the sublattice magnetization vectors are greatly reduced in length as they bend toward the field, in contrast to the molecular-field-theory prediction of constant length.

In Sec. 6 we discuss the effects of thermal expansion on the present results. Using the data of Gibbons,[21] the observed magnetic behavior is corrected to the case of fixed lattice parameters. In particular we estimate that the index β is raised by less than 1%, becoming

$$\beta=0.335\pm0.005,$$

while the constant D becomes

$$D=1.193\pm0.01.$$

2. EXPERIMENTAL TECHNIQUES

A. Temperature Control and Measurement

The low-temperature system is shown schematically in Fig. 1. A bath of liquid or solid nitrogen, which could be pumped down to 52°K, was contained in an outer Dewar. Immersed in this bath was an inner Dewar which in turn contained a heavy brass block. The MnF_2 sample, held by the NMR coil, was situated in a cavity in the block. Thermal contact between the sample and the block was promoted by filling the interior of the inner Dewar with helium at about 1 mm pressure. With the jacket (J) of the inner Dewar evacuated, the block tended toward a temperature equal to that of the bath with a time constant of about 10 h. This equilibrium temperature was raised by applying a suitable power input to a heater resistor embedded in the block. For example, at 50 mW input, the block tended to be about 10° warmer than the bath. Fine adjustments of the block's temperature were then achieved by manually altering the heater power; the temperature could be held constant to well within 1 mdeg by making these adjustments about every 10 min.

[21] D. F. Gibbons, Phys. Rev. **115**, 1194 (1959) and private communication.

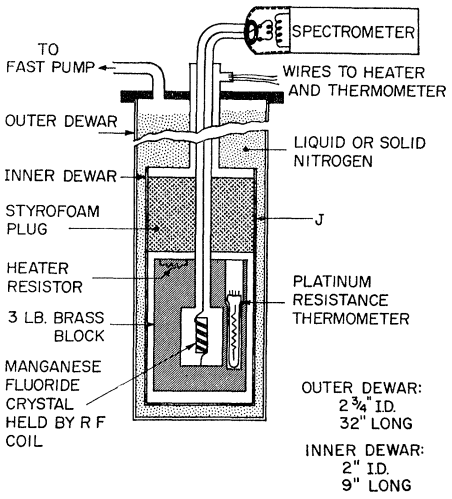

FIG. 1. Schematic diagram of the experimental apparatus. The inductive coupling arrangement shown was used with the Kushida spectrometer. When the Pound spectrometer was used it was connected directly to the coaxial line input.

Alternatively a reasonably linear temperature sweep of a few millidegrees per minute could be achieved by using a heater power somewhat higher or lower than that required to maintain a constant temperature.

Temperatures were measured with a four-lead platinum resistance thermometer (Leeds and Northrup Company, Type 8164). The readings were carefully corrected for the heating effect of the sensing current, a correction amounting to about 3 mdeg. It was quite important to correct for the effect of the applied field (magnetoresistance). This correction, which was determined experimentally, amounted to 5 mdeg at 8000 G. The possibility that the sample and the thermometer were not at exactly the same temperature was studied very carefully by varying each heat source within the experimental assembly and comparing the thermometer reading with that of the sample used as a nuclear resonance thermometer. In this way contributions to the steady-state temperature difference between the sample and the thermometer due to (a) the heater, (b) Ohmic losses in the NMR coil, and (c) eddy current heating of the brass block in the modulation field, were systematically investigated. These effects did not exceed 2 mdeg; they were corrected for. When the temperature rose or fell, the sample was observed to lag behind the thermometer. Great care was therefore taken to see that the steady state had been reached once the thermometer reading had stabilized. In runs in which the temperature was swept, the sweep rate was kept low enough so that the lag did not exceed a few millidegrees. This effect was always corrected for by taking the average of measurements employing up and down sweeps.

An absolute calibration of the platinum thermometer was made by using the sample cavity as the bulb of a nitrogen vapor pressure thermometer. Except for the removal of the sample and coil, the experimental ge-

ometry in the calibration runs was virtually identical to that in the NMR work. The calibration was carried out at numerous points from 55 to 77°K, using the nitrogen-vapor-pressure data of Armstrong[22] for the liquid and Keesom and Bijl[23] for the solid phase and triple point. The scatter in the calibration data was about ±5 mdeg. The resulting thermometer calibration curve was found to agree within 10 mdeg with one calculated from a helium-referenced Z function.[24] It is felt that the scale of absolute temperatures used here is in accord with the NBS low-temperature scale to within 20 mdeg or better.

B. Nuclear Resonance Techniques

Nuclear resonances below 41 Mc/sec were detected with a conventional Pound-Knight-Watkins spectrometer. Between 41 and 115 Mc/sec a VHF spectrometer of the type designed by Kushida[11] was employed. Since the transmission line leading to the sample coil was single ended and had a capacitance of ≈20 pF, the VHF spectrometer could not be connected directly. It was decided to try the inductive coupling scheme indicated in Fig. 1. In this method, both the primary and secondary circuits of the rf transformer are tuned to resonance. The operation of this system is rather complicated and has been described elsewhere.[3] It is not suitable when either frequency modulation or frequency sweep is used. When properly adjusted, the sensitivity obtained with it is comparable to that of the directly coupled system. Fortunately this adjustment could easily be optimized by observing the strong absorption due to the manganese spin-paramagnetic resonance at 77°K in fields $H_0 \approx 50$ G. With the inductive-coupling method, sensitivity to the nuclear dispersion χ' was sometimes apparent through a slight asymmetry in the observed line shapes. When this effect was noted, care was taken to correct for it in determining the true center of the line. Any resulting uncertainty in the frequency of the line center was very small, and has been included in the error estimates given with the data.

When the Pound spectrometer was used it was connected directly to the coaxial line input. Using both spectrometers, the frequency range from 22 to 115 Mc/sec was covered without making any changes inside the low-temperature system. A single 7-turn NMR coil was used. Nuclear resonances of width up to 3 Mc/sec could be detected.

Magnetic-field modulation amplitudes up to 130 G peak-to-peak were provided with a pair of 3-in. diam. Helmholtz coils placed inside the magnet gap. This rather strong modulation was required for observing the broad lines seen near T_N. (The brass block had to be slotted to minimize eddy-current heating which nevertheless amounted to as much as 50 mW.) Below T_N, the lines were usually traced out by sweeping the temperature and hence the internal field through resonance. Near and above T_N, a conventional magnetic-field sweep was used.

Magnetic field measurements between 170 and 8500 G were made with a proton resonance magnetometer whose readings were carefully corrected to give the field at the position of the MnF_2 sample.

C. The Sample. Sample Orientation

All the measurements were performed on a single sample of MnF_2 kindly provided by Dr. V. Jaccarino of the Bell Telephone Laboratories. It was a single crystal of nearly cylindrical shape, of diameter 0.23 in. and length 0.77 in., with the cylinder axis in the a' or [010] direction. It was mounted with the cylinder axis vertical. Thus the applied field could be positioned as desired in the ac plane.

In much of the work and particularly for the measurements reported in Sec. 4C, it was important to be able to align the external field $\mathbf{H}_0$ very accurately with respect to the c axis or alternatively to make a correction for any possible misalignment. The latter procedure was chosen, the precise orientation of the c axis being determined by NMR in a way we now outline.

The c axis is the direction of the field at the F^{19} nuclei for $T<T_N$ in zero-applied field. There are two nonequivalent F^{19} sites α and β which in zero applied field see oppositely directed local fields $\mathbf{H}_I(\alpha)$ and $\mathbf{H}_I(\beta)$, respectively. [See Fig. 2(b).] As it turned out, the sample was slightly cocked as shown in Fig. 2(a). The applied field could be brought most closely into coincidence with the c axis by rotating the magnet until $\mathbf{H}_0$ lay in a vertical plane containing the vector $\mathbf{H}_I(\alpha)$. This position, labeled X in Fig. 2(b), could be located to within ≈0.1° by maximizing the NMR frequency of the α site line. (This coincided, to within 0.1°, with the position of minimum β site NMR frequency.) It will be seen that if the cocking angle δ were zero, a small vertical field $\mathbf{H}_s$ would not produce a first-order change

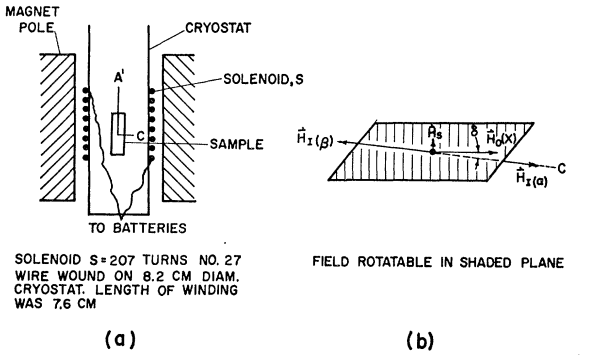

FIG. 2. Experimental method for determining the precise orientation of the c axis relative to the external field. The size of the MnF_2 sample has been greatly exaggerated.

[22] G. T. Armstrong, J. Res. Natl. Bur. Std. **53**, 263 (1954).
[23] W. H. Keesom and A. Bijl, Physica **4**, 305 (1937).
[24] G. K. White, *Experimental Techniques in Low Temperature Physics* (Oxford University Press, New York, 1959), p. 114.

in the NMR frequency of either site. Such a field was provided by a solenoid wound around the cryostat. This field was perpendicular to $\mathbf{H}_0$ to within 0.3°. By measuring the change in the α and β site NMR frequencies upon applying $\mathbf{H}_s$, two independent determinations of δ were made. Both sites gave $\delta=3.2\pm0.7°$, the consistency providing an additional check on the perpendicularity of $\mathbf{H}_s$ and $\mathbf{H}_0$. This result has been used to correct the data taken with $\mathbf{H}_0$ nominally along c, i.e., in position X, to the values that would have been observed for perfect alignment.

D. High-Pressure Techniques

For the measurement of the pressure dependence of the Néel point, a beryllium-copper high-pressure vessel and electrical plug designed by Benedek and described by him,[25] were used. Helium gas was used as the pressure-transmitting medium. Pressures up to 1500 atm were provided by a DA-4 pump made by the Harwood Engineering Company, Walpole, Massachusetts. Pressures were measured with a Carey-Foster bridge and Manganin gauge calibrated against a free piston gauge at Harwood. The absolute accuracy of the pressure measurements was ±4 atm.

The thermal mass of the high-pressure bomb was sufficiently large so that it could be used in place of the brass block in the temperature-control scheme of Fig. 1. The thermometer and heater were mounted in separate copper blocks strapped to the bomb. It was noted that the temperature of the thermally isolated bomb rose with increasing pressure and fell with decreasing pressure. This effect, which was roughly reversible, amounted to about 1 mdeg/atm. However, as leakage from the bomb was less than 2 atm/h, no difficulty was encountered in controlling the temperature once the desired pressure was reached.

3. THE EFFECT OF AN APPLIED FIELD ON THE RESONANCE LINES

In this section we present a phenomenological treatment of the behavior of NMR lines in an external field. A "law of corresponding states" model is discussed. A number of experimental tests will be presented in Sec. 4C, the model being found to provide a correct description of the observed behavior to within experimental error.

A. Phenomenological Treatment for a Weak Applied Field

It is convenient to formulate the discussion in terms of the "field at the nucleus" $\mathbf{H}_{\text{nucl}}$. This is related to the observed NMR frequency ν_{obs} by

$$\nu_{\text{obs}}=\gamma^{19}|\mathbf{H}_{\text{nucl}}|\,, \tag{7}$$

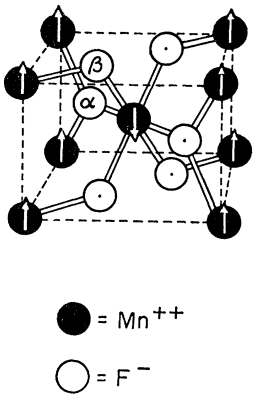

FIG. 3. The MnF_2 unit cell. In the antiferromagnetic state, the manganese spins are aligned up and down along the $c=[001]$ axis as shown.

where[26]

$$\gamma^{19}=4.007\text{ kc/G}.$$

In MnF_2 there are two nonequivalent F^{19} sites which we designate by α and β, as shown in Fig. 3. Below T_N, the manganese spins have the antiferromagnetic arrangement shown, and the fields at the nuclear sites for zero-external field can be written

$$\mathbf{H}_{\text{nucl}}(\alpha)=+\mathbf{1}_c H_I(T)\,;\quad \mathbf{H}_{\text{nucl}}(\beta)=-\mathbf{1}_c H_I(T)\,.$$

Here $\mathbf{1}_c$ is a unit vector in the c or [001] direction. The "internal field" $H_I(T)$ is thus the local field produced by the spontaneous magnetization of the manganese spin sublattices. It is proportional to the magnetization $M_0(T)$ of either sublattice in zero-external field. It is related to the zero-field NMR frequency $\nu_0(T)$ through the expression

$$\nu_0(T)=\gamma^{19}H_I(T)\,. \tag{8}$$

Or applying a weak external field $\mathbf{H}_0$ the local fields become

$$\begin{aligned}\mathbf{H}_{\text{nucl}}(\alpha)&=\mathbf{1}_c H_I(T)+\mathbf{H}_0+\mathbf{p}_\alpha(T)\cdot\mathbf{H}_0\,,\\ \mathbf{H}_{\text{nucl}}(\beta)&=-\mathbf{1}_c H_I(T)+\mathbf{H}_0+\mathbf{p}_\beta(T)\cdot\mathbf{H}_0\,.\end{aligned} \tag{9}$$

The terms on the far right of (9) represent the change in the local field due to the polarization of the manganese spins in the applied field. In the present work these terms amounted to between 6 and 9% of H_0. As these terms include the demagnetizing field, the tensors $\mathbf{p}_\alpha$ and $\mathbf{p}_\beta$ are somewhat dependent on the sample shape. The crystal structure is such that, for a spherical sample, the c axis is a principal axis of both tensors.[9] This will still be true for our cylindrical sample. Furthermore, the symmetry of the unit cell is such that the principal values along c are the same for both sites.[9] We denote this quantity by p_c. Moreover, we expect that the temperature dependence of p_c will be that of the parallel

[25] G. B. Benedek, *Magnetic Resonance at High Pressure* (Interscience Publishers Inc., New York, 1963), pp. 90–91.

[26] See, for example, N. F. Ramsey, *Molecular Beams* (Oxford University Press, Oxford, England, 1956).

susceptibility, i.e.,

$$p_c(T) \propto \chi_{II}(T). \tag{10}$$

In the present work p_c varied between 0.055 and 0.075 (see Fig. 9). Many measurements were made with $\mathbf{H}_0$ along c, in which case (9) becomes

$$\begin{aligned} \mathbf{H}_{\text{nucl}}(\alpha) &= \mathbf{1}_c\{H_I(T)+H_0[1+p_c(T)]\}, \\ \mathbf{H}_{\text{nucl}}(\beta) &= \mathbf{1}_c\{-H_I(T)+H_0[1+p_c(T)]\}. \end{aligned} \tag{11}$$

The quantity p_c is easily measured in the paramagnetic state where $H_I=0$ and hence

$$p_c=(H_{\text{nucl}}-H_0)/H_0=[\nu_{\text{obs}}/H_0-\gamma^{19}]/\gamma^{19}, \tag{12}$$

the applied field being along the c direction.

Many measurements were made with $\mathbf{H}_0$ along the $a=[100]$ direction. In this case the symmetry of the unit cell is such that the NMR frequencies of the α and β site lines are equal.[9] To describe this case it will be convenient to introduce a parameter p_a defined by

$$p_a \equiv |\mathbf{p}_\alpha \cdot \mathbf{1}_a + \mathbf{1}_a| - 1 = |\mathbf{p}_\beta \cdot \mathbf{1}_a + \mathbf{1}_a| - 1. \tag{13}$$

This quantity is easily measured in the paramagnetic state where

$$p_a=(H_{\text{nucl}}-H_0)H_0=[\nu_{\text{obs}}/H_0-\gamma^{19}]/\gamma^{19}, \tag{14}$$

the applied field being along the a direction. We expect that the temperature dependence of the transverse components of $\mathbf{p}_\alpha$ or $\mathbf{p}_\beta$ will be that of the perpendicular susceptibility $\chi_\perp$. It then follows that[27]

$$p_a(T) \propto \chi_\perp(T). \tag{15}$$

In the present work p_a was about 0.07 varying only slightly with temperature. Using (13) and (9), the magnitude of the field at either site may be written as

$$|\mathbf{H}_{\text{nucl}}| = \{[H_I(T)]^2+H_0^2[1+p_a]^2\}^{1/2}, \tag{16}$$

for $\mathbf{H}_0$ along [100].

B. Behavior in Stronger Fields. Law-of-Corresponding-States Model

Although Eq. (9) provides a correct account of the behavior encountered in weak fields, it cannot continue to apply as the field strength is increased, as we now show. We shall shortly see experimentally that the Néel temperature is actually a function of the applied field. For example, it will be shown that a field $H_0=10$ kG applied along [001] depresses the Néel point by 20 mdeg. Consider, then, the situation at 20 mdeg below the zero-field Néel point T_N. We shall find that at this temperature the spontaneous sublattice magnetization has already attained a value corresponding to an internal field $H_I=3$ kG. A 10-kG applied field will then completely destroy this spontaneous magnetization through the shift in the Néel point. Hence aside from its direct contribution to the local field, the effect of the applied field in this case is completely dominated by the shift of the Néel point.

A simple model for the effect of this shift on the sublattice magnetization $M(T)$ is provided by a "law of corresponding states." This "law" argues that as far as the effect of changing T_N is concerned, M is a function only of the reduced temperature, i.e.,

$$M=F(T/T_N).$$

A similar assumption has been employed in analyzing the effect of hydrostatic pressure on the magnetization.[11]

The effect of changing T_N is conveniently represented in terms of an equivalent change in the actual temperature T. Thus, writing the shift in the Néel point as

$$\delta T_N = T_N(\mathbf{H}) - T_N,$$

we write

$$\begin{aligned} M[T,T_N(\mathbf{H})] &= F\left[\frac{T}{T_N+\delta T_N}\right] \approx F\left[\frac{T-(T/T_N)\delta T_N}{T_N}\right] \\ &= M[T-\delta T_N(T/T_N),\, T_N]. \end{aligned}$$

Hence we are led to modify Eqs. (9) by replacing[28] T by $T-(T/T_N)\delta T_N$. We then have

$$\begin{aligned} \mathbf{H}_{\text{nucl}}(\alpha) &= \mathbf{1}_c H_I[T-(T/T_N)\delta T_N]+\mathbf{H}_0+\mathbf{p}_a(T)\cdot\mathbf{H}_0, \\ \mathbf{H}_{\text{nucl}}(\beta) &= -\mathbf{1}_c H_I[T-(T/T_N)\delta T_N] \\ &\quad +\mathbf{H}_0+\mathbf{p}_\beta(T)\cdot\mathbf{H}_0. \end{aligned} \tag{17}$$

These equations provide the basis for our analysis of the NMR data.

It follows from symmetry that the Néel temperature is an even function of the applied field. We shall in fact assume that δT_N is proportional to H_0^2. We now consider two special cases.

(i) *Applied Field along [100]*

The Néel point shift can be written as

$$\delta T_N = -K_a H_0^2. \tag{18}$$

Then, using (13) and (17), the magnitude of the local field at either site is

$$\begin{aligned} H_{\text{nucl}} = \{&[H_I(T+K_a H_0^2 T/T_N)]^2 \\ &+H_0^2[1+p_a(T)]^2\}^{1/2}. \end{aligned} \tag{19}$$

(ii) *Applied Field along [001]*

The Néel point shift can be written as

$$\delta T_N = -K_c H_0^2. \tag{20}$$

[27] In writing Eq. (15) we have dropped some terms of order p_a^2. The error thereby introduced is entirely negligible.

[28] The temperature dependence of the p tensors is so slight that it is not necessary to make this replacement in the terms on the far right in (9).

Then

$$\mathbf{H}_{\rm nucl}(\alpha)=\mathbf{1}_c\{H_I(T+K_cH_0^2T/T_{\rm N})+H_0[1+p_c(T)]\},$$
$$\mathbf{H}_{\rm nucl}(\beta)=\mathbf{1}_c\{-H_I(T+K_cH_0^2T/T_{\rm N})+H_0[1+p_c(T)]\}. \quad (21)$$

If $|\delta T_{\rm N}|\ll T_{\rm N}-T$ we can write (21) in the form

$$|\mathbf{H}_{\rm nucl}(\alpha)-\mathbf{H}_0|=H_I(T)+p_cH_0+\delta_cH_0^2,$$
$$|\mathbf{H}_{\rm nucl}(\beta)-\mathbf{H}_0|=H_I(T)-p_cH_0+\delta_cH_0^2, \quad (22)$$

where

$$\delta_c=K_c(T/T_{\rm N})dH_I/dT. \quad (23)$$

It is instructive to write this result in a slightly different way. Let $\delta H_{\rm nucl}{}^{(2)}=\delta_cH_0^2$ denote the second-order change in the field at the α-site nucleus due to the field. Then by (20)

$$\delta H_{\rm nucl}{}^{(2)}=-(T/T_{\rm N})(dH_I/dT)\delta T_{\rm N}.$$

Since $\delta T_{\rm N}$ and dH_I/dT are negative, $\delta H_{\rm nucl}{}^{(2)}$ is negative. Physically we may say that as H_0 is increased, the sample is brought closer to its Néel point, thereby reducing the portion of the local field associated with the antiferromagnetism of the manganese spins.

4. EXPERIMENTAL DATA

A. The Pressure Dependence of $T_{\rm N}$

For reasons to be discussed in II, the NMR signal strength decreased very rapidly as $T_{\rm N}$ was approached from the paramagnetic side. This fade-out was particularly sharp with H_0 along [100]. With this field orientation, the NMR lock-in detector output was monitored as the temperature was swept slowly. The point T_D at which the signal disappeared into the noise could be pinned down to within about a millidegree. Actually, T_D depended slightly on the NMR sensitivity and was a few millidegrees lower than $T_{\rm N}$. (This was due to the persistence of the paramagnetic state lines into the antiferromagnetic state, an effect to be discussed in II.) It is clear, however, that the pressure dependence of T_D is the same as that of $T_{\rm N}$, i.e.,

$$T_{\rm N}(P)-T_{\rm N}(0)=T_D(P)-T_D(0). \quad (24)$$

In Fig. 4 we plot the right-hand side of (24) for five pressures P. We find that to well within the indicated uncertainties the shift of $T_{\rm N}$ with pressure is linear and

$$dT_{\rm N}/dP=303\pm3 \text{ mdeg/1000 kg/cm}^2.$$

This result agrees well with the estimate of Benedek and Kushida[11] obtained by a quite different method.

B. The Field Dependence of $T_{\rm N}$

On account of the frequency dependence of the sensitivity of the NMR system, the shift of the disappearance point did not provide a satisfactory measure of the field dependence of $T_{\rm N}$. Accordingly, the following procedure was adopted. The temperature dependence of the NMR signal strength was measured at a field $H_0=5.4$ kG. Then, another set of measurements was made at $H_0=8.25$ kG. A scale factor was applied to the second set of measurements so as to bring the resulting curve of signal strength versus temperature parallel to the curve obtained from the first set. The displacement in temperature of one set of measurements relative to the other was taken as the shift of the Néel point.

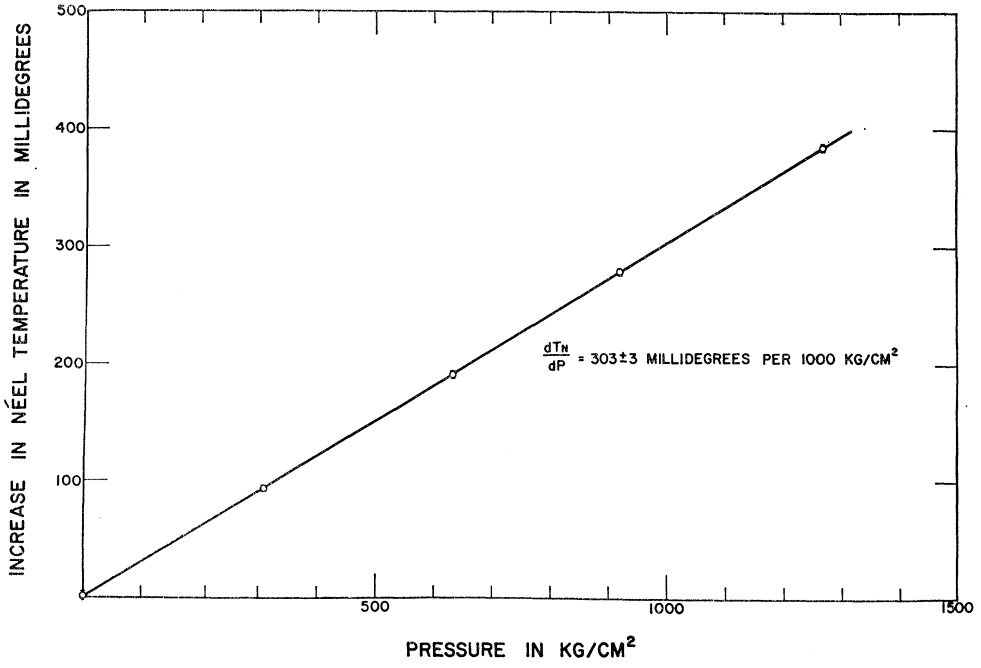

FIG. 4. The pressure dependence of the Néel temperature.

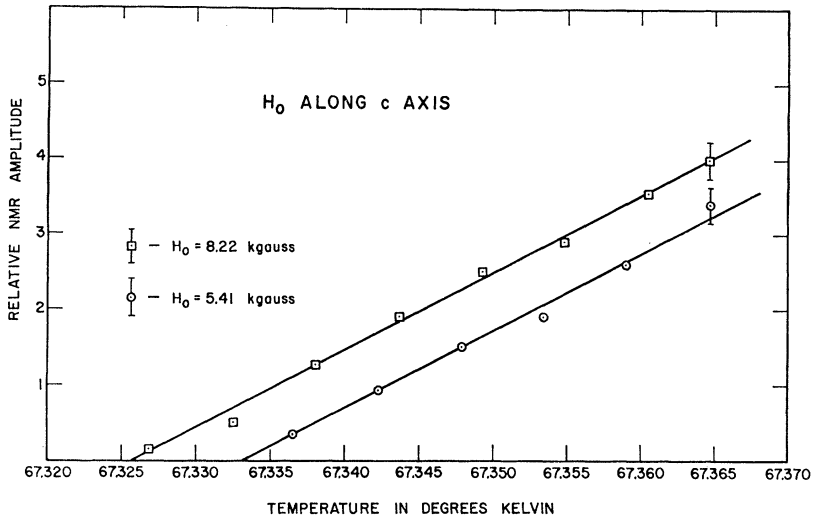

FIG. 5. F^{19} signal amplitude versus temperature just above T_N in an applied field directed along the c axis. Upper and lower curves are for H_0 =8.22 and 5.41 kG, respectively. The depression of the Néel point with increased H_0 is apparent.

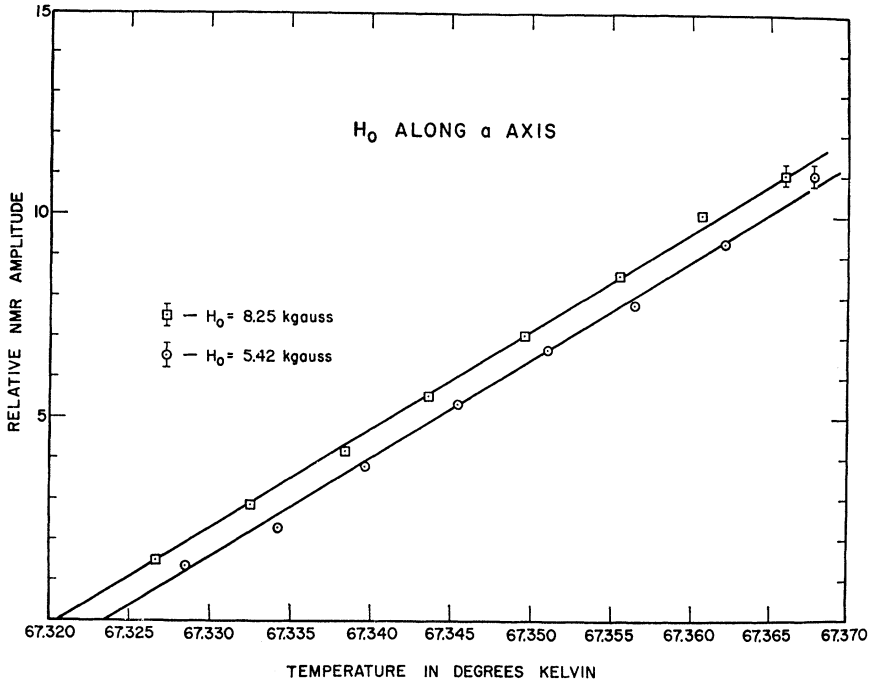

FIG. 6. F^{19} signal amplitude versus temperature just above T_N in an applied field directed along the a axis. Upper and lower curves are for H_0=8.25 and 5.42 kG, respectively. The depression of the Néel point with increased H_0 is apparent.

This procedure was first followed for H_0 along [001], the results being displayed in Fig. 5, and then with H_0 along [100], the results being shown in Fig. 6. We find that the Néel point is depressed by the field as summarized in Table I. The values of the constants K_c and K_a are computed on the assumption that the Néel-point shift is quadratic in H_0.

TABLE I. The field dependence of T_N.

Field direction	T_N(8.25 kG) $-T_N$(5.4 kG) (mdeg)	K, assuming Eqs. (18) and (20) (mdeg/kG²)
c=[001]	−7.5±1	−0.195±0.03
a=[100]	−2.8±1	−0.075±0.03

C. Verification of the Law-of-Corresponding-States Model

(i) *Applied Field along [001]*

An experiment was carried out at T=65.560°K to determine the precise dependence of H_{nucl} on H_0 with $\mathbf{H}_0$ along [001]. The data have been corrected for the misalignment of the MnF_2 sample according to the pro-

cedures described in Sec. 2 and Appendix A. The results are shown in Fig. 7. Here we plot $|\mathbf{H}_{\text{nucl}}-\mathbf{H}_0|$ versus H_0 for both F^{19} sites. These data are now fitted to Eqs. (22) as follows. The value of p_c is chosen so that the departures from the straight lines of slope $\pm p_c$ are the same for both sites. The lines are drawn to have a common intercept H_I. When now the data is replotted in the form $|\mathbf{H}_{\text{nucl}}-\mathbf{H}_0-p_c\mathbf{H}_0|$ versus H_0^2 as in Fig. 8, δ_c is the slope of the graph. Thus we find

$$\begin{aligned} H_I(65.560°\text{K}) &= 14\,280\pm4\text{ G},\\ p_c(65.560°\text{K}) &= 0.0715\pm0.005,\\ \delta_c(65.560°\text{K}) &= -(49\pm5)\times10^{-8}\text{ G}^{-1}. \end{aligned} \tag{25}$$

The experimental uncertainties shown in Fig. 7 and Fig. 8 correspond to 5% of the linewidth or, equivalently, to an uncertainty of 1.5 mdeg in the measured temperature. To give an idea of the effect of making the misalignment correction we state that the values of p_c and $|\delta_c|$ deduced from the uncorrected data are, respectively 3 and 30% smaller than those given in (25). In this connection, we note that misalignment, or any mechanism through which H_0 produces at the nucleus a field not colinear with [001], will give rise to a spurious quadratic term in the observed H_{nucl} versus H_0 data. Thus we should consider the possibility that terms are present in the **p** tensors which mix the [001] and transverse directions. Demagnetizing effects would produce such terms if the sample's cylindrical axis were not along [100]. Conservative estimates of this and other possible mechanisms fail by at least an order of magnitude to account for the observed value of δ_c. Moreover, it should be noted that any such spurious quadratic effect would necessarily have a positive sign while the observed effect has a negative sign, i.e., δ_c is negative.

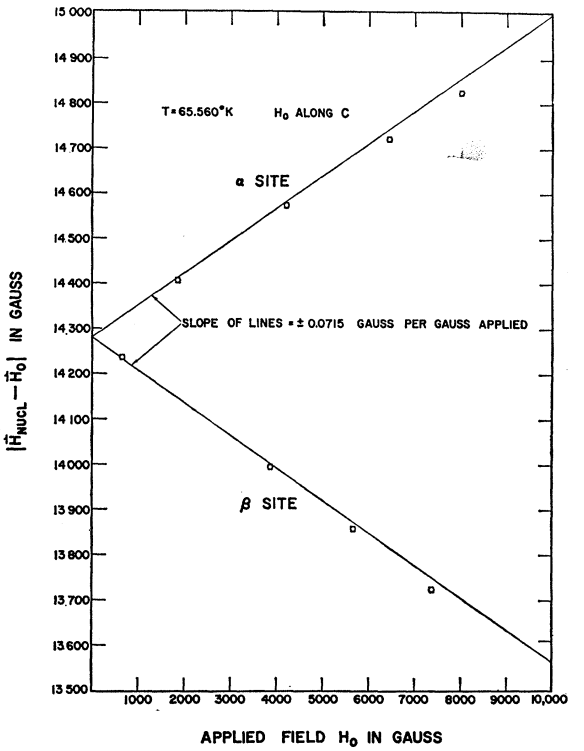

FIG. 7. Contribution of the manganese spins to local field as a function of an external field H_0 applied along the c axis. If the sublattice magnetizations were linear in H_0, the data for the α and β site resonances would lie on straight lines of equal and opposite slopes.

That the observed quadratic effect is indeed associ-

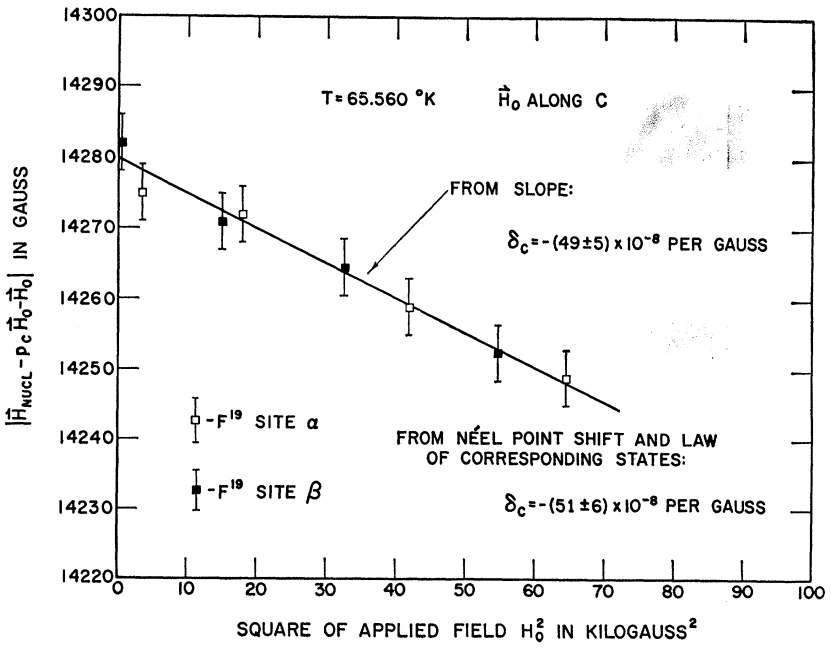

FIG. 8. Field at the nucleus minus the term proportional to H_0 versus H_0^2 for the data of Fig. 7. The quantity δ_c is defined in Eq. (22). Its value agrees well with the value calculated from the measured field dependence of the Néel temperature using Eq. (23).

ated with the shift of the Néel point may be shown by computing δ_c according to the law-of-corresponding-states model using Eq. (23). From results to be given in Sec. 4D we find that

$$(dH_I/dT)_{65.560°K} = -2.67 \text{ G/mdeg},$$

while K_c is given in Table I. We then find

$$\delta_c(65.560°K) = -(51 \pm 7) \times 10^{-8} \text{ G}^{-1}, \quad (26)$$

which agrees well with the observed result (25).

In summary, we find experimentally that H_{nucl} is a somewhat nonlinear function of the applied field H_0. This nonlinearity is to be attributed to the effect of the field in depressing the Néel point by an amount proportional to H_0^2. Upon using the independently measured value of the Néel point shift reported in Sec. 4B, we obtain a quantitative prediction for the nonlinear behavior which is in good agreement with experiment.

(*ii*) *The Temperature Dependence of p_c and p_a*

In the antiferromagnetic state, in addition to the measurement just described, p_c was also determined at 63.134°K by measuring H_{nucl} at two values of H_0, taking δ_c to be given by (23). In the paramagnetic state p_c was determined from observations made at a number of different temperatures using (12). These experimental results are shown by the open circles in Fig. 9.

The temperature dependence of p_c may also be computed from magnetic susceptibility data. The results, shown by the black circles in Fig. 9, were obtained as follows. From Stout and Griffels' measurements[12] of the anisotropy $\chi_{II} - \chi_\perp$, and the value[29] $\chi_{II}(T_N) = 23.7 \times 10^{-3}$ per mole, $\chi_{II}(T)$ was calculated on the assumption that $\chi_\perp(T) = \chi_\perp(T_N)$ below T_N. Using $p_c(T_N) = 0.0756$, $p_c(T)$ was then computed from Eq. (10). We see in Fig. 9 that the NMR results are consistent with these determinations, indicating the correctness of the assumption of constant $\chi_\perp$. (In fact, the susceptibility measurements of Bizette and Tsai[13] indicate that $\chi_\perp$ changes by less than a percent from T_N to 50°K.)

In the paramagnetic state, p_a was determined from observations made at a number of temperatures using (14). The results are shown in Fig. 9 by the triangles. No direct determinations of p_a were made in the antiferromagnetic state. On account of (15), we may expect that p_a will remain constant below T_N. This has been indicated in Fig. 9 by the dotted line. This extrapolation is sufficient for the purposes of the present work, where all measurements with H_0 along [100] were made above 67.2°K.

(*iii*) *Comparison of Data for* $\mathbf{H}_0$ *along [001] and [100]*

The internal field H_I or equivalently the zero-field NMR frequency $\nu_0 = \gamma^{19} H_I$ can now be calculated from the NMR data taken in an applied field oriented either

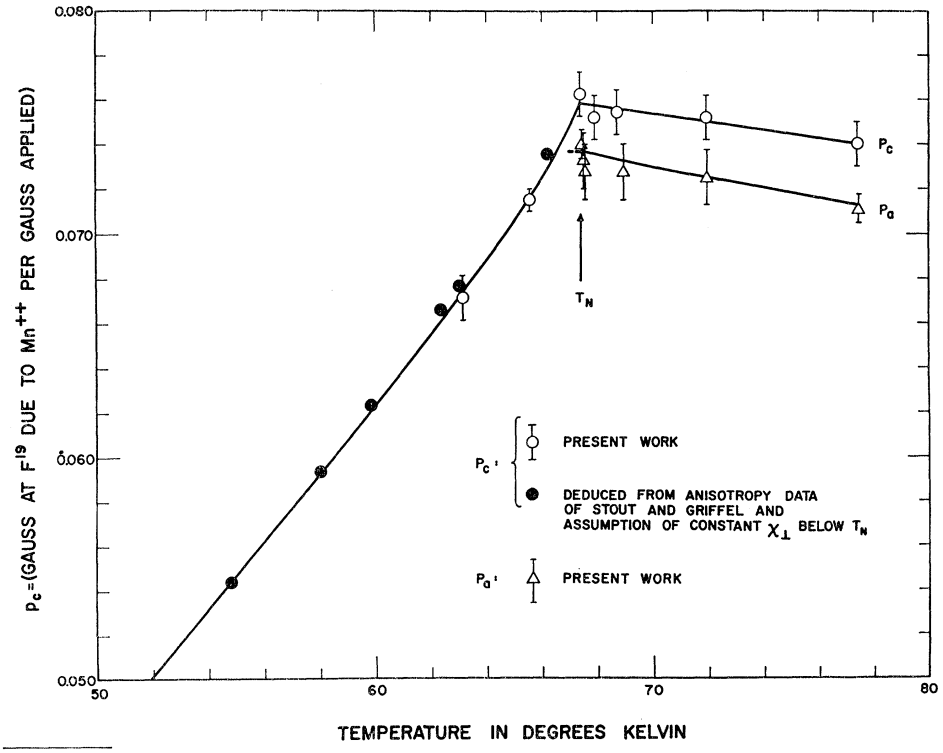

FIG. 9. The temperature dependence of p_c and p_a. These quantities, which essentially represent the change in the manganese spin contribution to the local field per unit applied field, reflect the temperature dependences of χ_{II} and $\chi_\perp$, respectively.

[29] W. J. Dehaas, B. H. Schultz, and J. Koolhaas, Physica 7, 57 (1940).

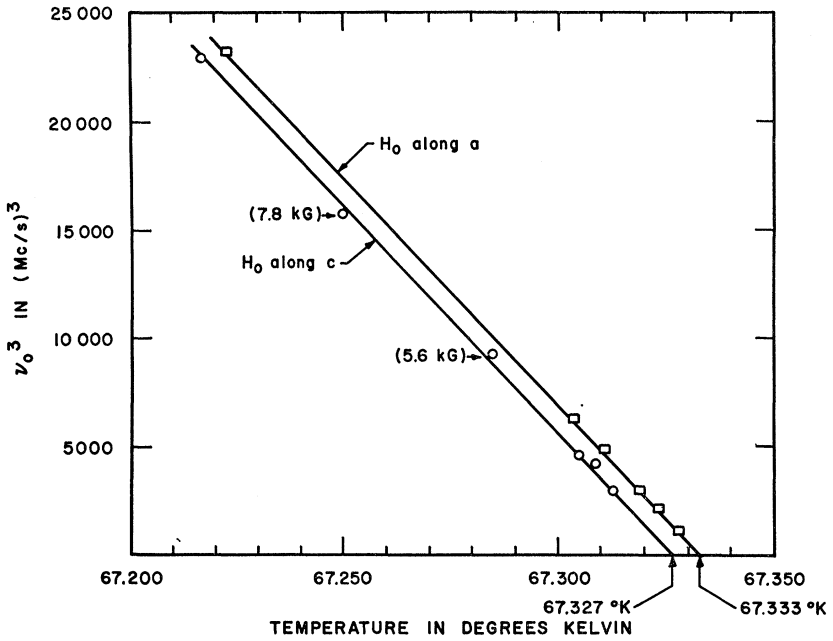

FIG. 10. The temperature dependence of the cube of the zero-field NMR frequency calculated using Eqs. (27) and (28) from the NMR data taken in an applied field H_0 oriented along c (lower line) or a (upper line). These calculations do *not* correct for the shift in the Néel point. This shift is readily apparent in the figure. Except for the two labeled points, all the measurements were made with $H_0 = 6.9$ kG.

along [001] or [100]. To obtain the temperature dependence of ν_0 precisely we must take the shift of the Néel point into account, i.e., we must use Eqs. (19) and (21) in interpreting the data. However, to demonstrate the effect of this shift we shall first intentionally neglect it, using Eqs. (11) and (16) to derive $\nu_0(T)$ in terms of the observed NMR frequency. Thus for measurements made with $\mathbf{H}_0$ along [001], Eqs. (7), (8), and (11) yield[30]

$$\nu_0(T) = \nu_{\rm obs} \mp (1+p_c)\gamma^{19}H_0, \qquad (27)$$

the minus and plus sign applying, respectively, to the α and β site resonances. For the measurements made with $\mathbf{H}_0$ along [100] Eqs. (7), (8), and (16) give

$$\nu_0(T) = [\nu_{\rm obs}^2 - (1+p_a)^2(\gamma^{19}H_0)^2]^{1/2}. \qquad (28)$$

In Fig. 10 we plot the cubes of the ν_0 values thus obtained versus temperature for $67.217°\text{K} < T < 67.328°\text{K}$. The circles and squares correspond respectively to measurements made with $\mathbf{H}_0$ along [001] and [100]. Except for the two labelled points, all these measurements were made in fields $H_0 = 6.9 \pm 0.5$ kG. We see that for each field orientation ν_0^3 decreases linearly with increasing temperature. By extrapolating over the last few millidegrees we obtain the Néel temperatures for each field orientation:

$$T_{\rm N}(c, 6.9\text{ kG}) = 67.327°\text{K},$$
$$T_{\rm N}(a, 6.9\text{ kG}) = 67.333°\text{K}. \qquad (29)$$

This is in accord with the results of Sec. 4B where we saw that the Néel point depression is larger with H_0 along c. In fact, using Table I we compute that

$$T_{\rm N}(a, 6.9\text{ kG}) - T_{\rm N}(c, 6.9\text{ kG}) = 6\text{ mdeg},$$

in exact accord with (29). This provides additional evidence in favor of the model described in Sec. 3, namely that the effect of an external field on each sublattice is, in addition to a field-proportional polarization described by the susceptibility, a reduction in the length of the component of the magnetization along the antiferromagnetic axis by an amount that corresponds to the Néel-point shift.

D. The Temperature Dependence of the Zero-Field NMR Frequency

We now take the Néel point shift into account in obtaining $\nu_0(T)$ from the NMR data. For measurements made with $\mathbf{H}_0$ along [001] Eqs. (7), (8), and (21) yield[30]

$$\nu_0(T + K_c H_0^2 T/T_{\rm N}) = \nu_{\rm obs} \mp (1+p_c)\gamma^{19}H_0 \qquad (30)$$

in place of (27). For measurements made with $\mathbf{H}_0$ along [100], Eqs. (7), (8), and (19) give

$$\nu_0(T + K_a H_0^2 T/T_{\rm N}) = [\nu_{\rm obs}^2 - (1+p_a)^2(\gamma^{19}H_0)^2]^{1/2} \qquad (31)$$

in place of (28). These relations have been applied to the observed NMR frequencies. The results are listed in Table II. For each measurement we list the right-hand side of (30) or (31), together with the appropriate "corrected temperature" $T + KH_0^2 T/T_{\rm N}$. (The difference between this and the actual temperature was calculated using the values of K_a and K_c listed in Table I. This difference did not exceed 13 mdeg.) The first twelve entries correspond to the points plotted in

[30] For the case of the β site resonance we have assumed in writing (27) that the magnitude of the internal field exceeds that of the applied field. This was the case in practice.

TABLE II. Temperature dependence of the zero-field F^{19} resonance frequency.

Temperature in °K	Frequency in Mc/sec
67.332±0.002	8.0
67.326±0.003	10.2
67.322±0.003	11.4
67.322±0.004	11.3
67.315±0.003	12.7
67.314±0.004	13.4
67.313±0.004	13.2
67.307±0.003	14.6
67.291±0.003	16.6
67.262±0.003	19.9
67.227±0.003	22.5
67.226±0.004	22.6
67.202±0.004	24.0
67.188±0.004	25.0
67.139±0.004	27.5
67.125±0.004	27.8
67.117±0.004	28.3
67.104±0.004	28.7
67.098±0.004	29.14
66.987±0.004	33.12
66.842±0.003	37.37
66.635±0.002	41.95
66.334±0.002	47.20
66.195±0.002	49.345
65.891±0.002	53.38
65.560±0.002	57.22
65.325±0.002	59.66
65.266±0.003	60.22
64.589±0.015	66.19
63.184±0.010	75.90
63.157±0.004	76.16
62.510±0.006	79.84
61.535±0.015	84.84
60.577±0.008	89.14
59.146±0.010	94.91
57.724±0.015	99.92
56.653±0.010	103.30
56.080±0.005	105.04
56.063±0.002	105.10
53.915±0.010	111.04
52.983±0.020	113.38
52.272±0.020	115.10

Fig. 11. The remaining points were all taken with $\mathbf{H}_0$ along [001]. All experimental uncertainties have been expressed in terms of an equivalent uncertainty in the temperature. These errors include the uncertainty in the values of p_a and p_c used in computing ν_0 from ν_{obs}.

Thus, according to the considerations presented above, the data of Table II represent the temperature dependence of the F^{19} resonance frequency $\nu_0(T)$ that would have been observed in zero-applied field had such measurements been technically feasible.

In Fig. 11 we plot $\nu_0(T)$ versus T. For comparison we include a curve of $\nu_0(T)$ computed from Eqs. (2) and (3) on the molecular field model using a spin $\frac{5}{2}$ Brillouin function for the sublattice magnetization.[31]

In Fig. 12 we plot $[\nu_0(T)]^3$ versus T for 65.560°K $<T<$67.332°K. Thus we find that the data very accurately fit an expression of the form

$$\nu_0(T)/\nu_0(0)=D(1-T/T_N)^{1/3} \tag{32}$$

where

$$D=1.200\pm0.004, \quad T_N=(67.336\pm0.003)°\text{K}, \tag{33}$$

and[9] $\nu_0(0)=159.978$ Mc/sec.

We would like to be able to plot all of the data of Table II in a form which illustrates the critical behavior (32), together with the departures from this law which must take place at lower temperatures. In addition we wish to show with what precision the data define the exponent β in the more general expression

$$\nu_0(T)/\nu_0(0)=D(1-T/T_N)^{\beta}. \tag{34}$$

To accomplish these aims we put

$$\Delta T=T_N-T-T_N\{(1/D)[\nu_0(T)/\nu_0(0)]\}^{1/\beta}. \tag{35}$$

This quantity represents the departure from linearity of a $\nu^{1/\beta}$ versus T plot. (The value of D is chosen so that ΔT vanishes at about $0.9T_N$.) In Fig. 13 we plot $\Delta T/T_N$ versus T/T_N for five choices of β. The region in which (34) applies is the one in which this plot has no curvature.

Figure 13 shows that on a scale of accuracy corresponding to a precision of about a part in 10^4 in the temperature, Eq. (34) fits the data with

$$\beta=0.333\pm0.003,$$

for reduced temperatures above 0.92. Noting from Table II that the data start at about 4 mdeg below T_N, we see that (32) fits with remarkable accuracy for

$$0.92<T/T_N<0.99993.$$

Our discussion has shown that a power law very accurately fits the MnF_2 data. Recently, Edwards[32] has shown that a different mathematical expression describes the critical behavior of the fluids He^4 and He^3. For our magnetic problem, this type of behavior would imply that, on letting $X=\nu(T)/\nu(0)$, the function

$$f=X^2/(1-\ln X)$$

should vary linearly with temperature.[32] Accordingly we have plotted the data of Table II in this form. For the range $0.92<T/T_N<0.99993$, a curve of f versus T is found to depart from the straight line drawn through its ends by roughly 40 times the scatter of the data points. For the range $0.97<T/T_N<0.99993$, the departure from linearity is about ten times the scatter. We conclude that this type of expression provides a rather poor description of the behavior of MnF_2.

5. INTERPRETATION OF THE DATA ON THE MOLECULAR-FIELD THEORY

A. The Predicted Behavior

We first summarize the results to be derived in Sec. 5B concerning the behavior predicted on the molecular-

[31] L. P. Schmid and J. S. Smart, U. S. Naval Ordnance Laboratory, White Oak, Maryland, Navord Report 3640 (unpublished).

[32] M. H. Edwards, Phys. Rev. Letters **15**, 348 (1965).

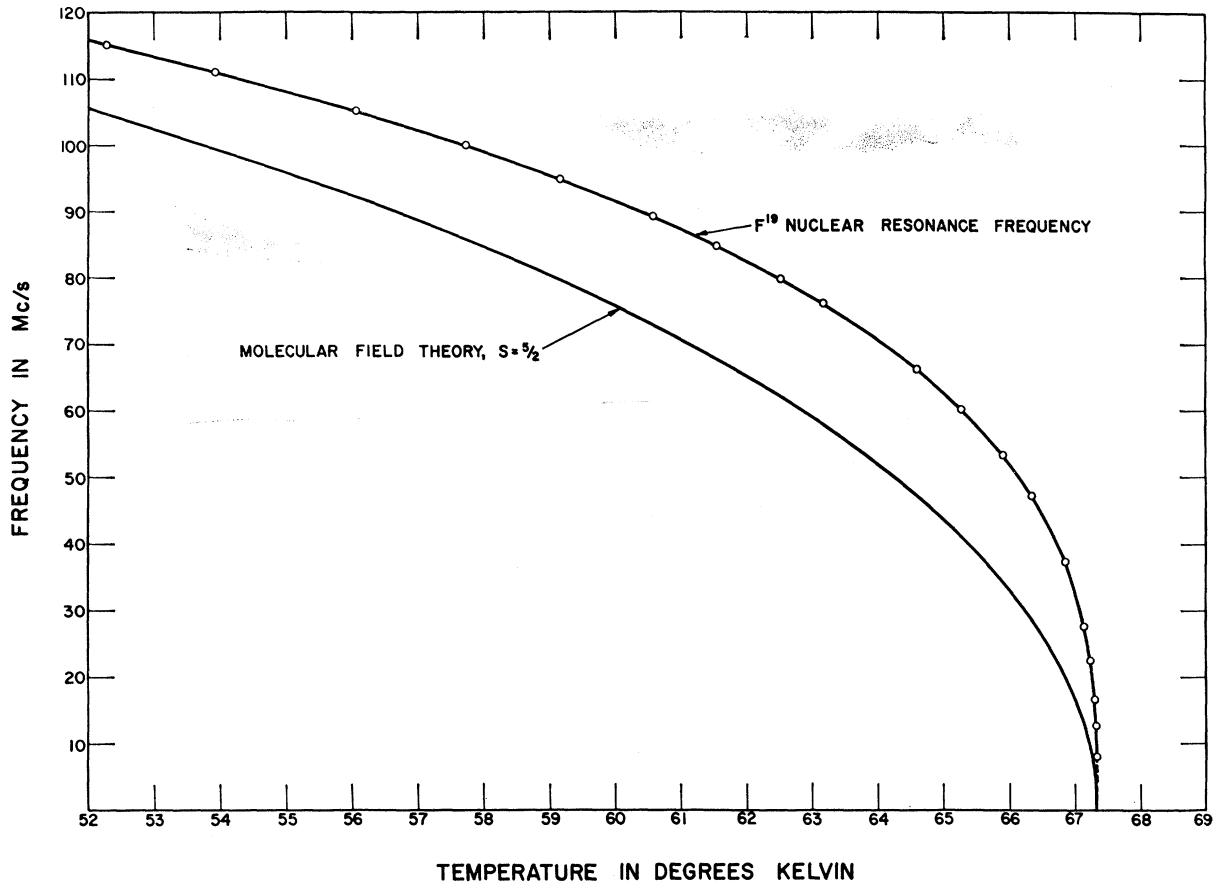

FIG. 11. Temperature dependence of the zero-field F^{19} NMR frequency in the range $52°K<T<T_N$. The circles greatly exaggerate the size of the experimental uncertainties. The lower curve is computed using the molecular field theory and $\nu_0(0°K)=159.98$ Mc/sec.

field model of a two-sublattice spin-S antiferromagnet with a uniaxial anisotropy, in fields below the threshold for spin-flopping.

(i) The Critical Behavior in Zero External Field

Below the Néel point the sublattice magnetization vectors $\mathbf{M}_+$ and $\mathbf{M}_-$ point, respectively up and down along the preferred axis. As is well known, the temperature dependence of their length $M_0(T)$ near T_N is given by

$$\begin{aligned} M_0(T)/M_0(0)&=D(T)(1-T/T_N)^{1/2}, \quad T\leq T_N \\ &=0, \qquad\qquad\qquad T\geq T_N. \end{aligned} \tag{36}$$

In Eq. (36), $D(T)$ is a slowly varying function which for our purposes may be taken equal to its value D_N at the Néel point

$$\begin{aligned} D_N&=[(10/3)(S+1)^2/(2S^2+2S+1)]^{1/2} \\ &=1.485 \quad \text{for} \quad S=\tfrac{5}{2}. \end{aligned} \tag{37}$$

Equation (36) is analogous to the square-root law

$$\rho_{liq}-\rho_{gas}\propto(T_c-T)^{1/2}$$

obtained by applying the van der Waals equation of state, and the Maxwell construction in calculating the densities of the coexisting phases near fluid critical points.[33]

(ii) The Critical Behavior in an Applied Field

Our results are conveniently formulated in terms of the sum and difference of the sublattice magnetization vectors. The sum, i.e., the bulk magnetization, is given by

$$\mathbf{M}_+(T,\mathbf{H})+\mathbf{M}_-(T,\mathbf{H})=\chi(T)\cdot\mathbf{H}\approx\chi_N\mathbf{H}. \tag{38}$$

The temperature dependence[18] of the susceptibility tensor χ is well known. We point out here that χ varies rather slowly and, for the case of MnF_2, is practically isotropic at and above T_N. As indicated in Eq. (38) it will suffice here to regard χ as a constant scalar χ_N. The experimental value[29] of χ_N for MnF_2 may be expressed as

$$\tfrac{1}{2}\chi_N/M_0(0)=8.48\times10^{-7}/\text{G}. \tag{39}$$

[33] See, for example, K. Huang, *Statistical Mechanics* (John Wiley & Sons, Inc., New York, 1963), pp. 40–46.

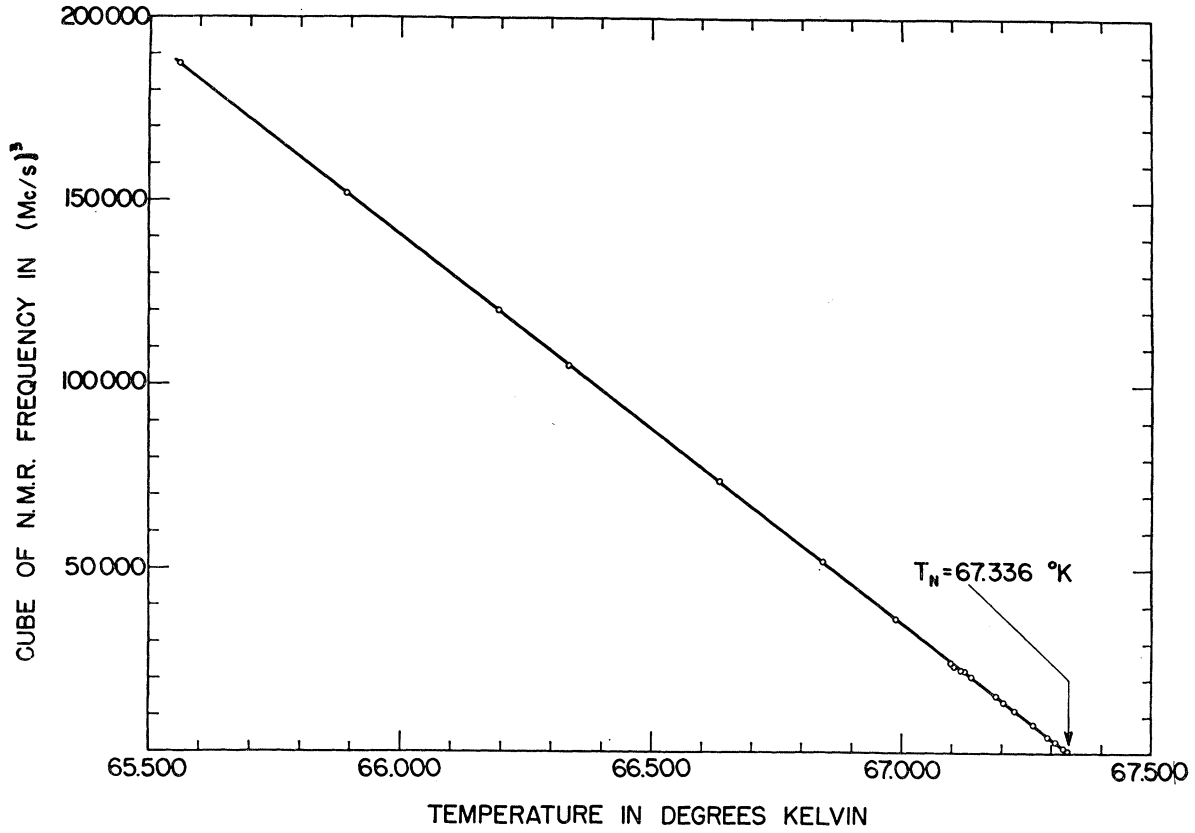

FIG. 12. Temperature dependence of the cube of the zero-field F^{19} NMR frequency for the first 1.8°K below T_N. The points lie on the straight line shown to within the experimental uncertainty of about 5 mdeg. These points are calculated from measurements made in an applied field using Eqs. (30) and (31). These equations include small corrections for the shift in the Néel point produced by the field.

The difference in the sublattice magnetizations near T_N is given by

$$\begin{aligned}&\mathbf{M}_+(T,\mathbf{H})-\mathbf{M}_-(T,\mathbf{H})\\&=\mathbf{1}_c 2M_0(0)D(T,\mathbf{H})[1-T/T_N(\mathbf{H})]^{1/2}, \quad T\leq T_N(\mathbf{H})\\&=0 \qquad\qquad\qquad\qquad\qquad\qquad\qquad\qquad , \quad T\geq T_N(\mathbf{H}).\end{aligned} \tag{40}$$

Here, $\mathbf{1}_c$ is a unit vector in the preferred direction, and $D(T,\mathbf{H})$ is a slowly varying function which for our purposes may be taken equal to D_N. The field-dependent Néel point $T_N(\mathbf{H})$ is given by

$$\begin{aligned}T_N(\mathbf{H})=T_N-[\tfrac{1}{2}\chi_N/M_0(0)]^2\\\times(T_N/D_N{}^2)(1+2\cos^2\phi)H^2,\end{aligned} \tag{41}$$

where ϕ is the angle between $\mathbf{H}$ and the preferred axis. For $0\neq\phi\neq\pi/2$, Eqs. (40) and (41) are valid if we assume that the applied field is not strong enough to shift the Néel point by an amount comparable to the anisotropy energy expressed as a temperature. The derivation of (40) and (41) also assumes that the contribution of the anisotropy to the molecular field is linear in $\mathbf{M}_+$ and $\mathbf{M}_-$. These assumptions can be dropped for the special cases $\phi=0$ and $\phi=\pi/2$.

Equations (38), (40), and (41) completely predict the behavior of the sublattices in the critical region. However, it is useful to restate these results in a different form. By combining (38) and (40), taking $D(T,\mathbf{H})=D_N=D(T)$, and comparing with (36) we find

$$\mathbf{M}_\pm(T,\mathbf{H})=\tfrac{1}{2}\chi\cdot\mathbf{H}\pm M_0(T-\delta T_N)\mathbf{1}_c, \tag{42}$$

where

$$\delta T_N=T_N(\mathbf{H})-T_N.$$

Equation (42) is analogous to Eqs. (17) of Sec. 3. It shows, as did the NMR experiments, that the effect of an external field on each sublattice is, in addition to a field-proportional term corresponding to the susceptibility, a reduction in the length of the component of the magnetization along the preferred axis by an amount attributable to the shift in the Néel point.

These results will now be specialized to the two applied field orientations used in the NMR experiments. For $\mathbf{H}$ along the preferred axis, we expand $M_\pm(T,H)$ in a power series in H:

$$M_\pm(T,H)=\pm M_0(T)+\delta M_\pm{}^{(1)}+\delta M_\pm{}^{(2)}+\cdots, \tag{43}$$

where $\delta M_\pm{}^{(1)}$ and $\delta M_\pm{}^{(2)}$ are, respectively linear and quadratic in H. The linear term corresponds to the

ordinary susceptibility and may be written

$$\delta M_{\pm}^{(1)} = \tfrac{1}{2}\chi_{\parallel}(T)H.$$

Just below the Néel point, the quadratic term is given by

$$\delta M_{\pm}^{(2)} = \mp \delta T_N dM_0/dT. \tag{44}$$

This result follows from Eqs. (38) and (40) and the fact that the function $D(T,H)$ and its derivatives are well behaved. Equation (44) is valid asymptotically as $T \to T_N$, where it is equivalent to the result (23) derived from the law of corresponding states model. An exact expression for $\delta M_{\pm}^{(2)}$ given elsewhere[3] shows that the law of corresponding states fails well below T_N, but provides a good approximation for $T/T_N > 0.9$.

When H is increased to the point where δT_N becomes comparable to $T_N - T$, the power series (43) is inadequate. $\mathbf{M}_+$ grows while $\mathbf{M}_-$ shrinks, reverses sign, and eventually coincides with $\mathbf{M}_+$ along the direction of $\mathbf{H}$. The system has then been driven into the paramagnetic state. This is illustrated in Fig. 16(a).

For $\mathbf{H}$ perpendicular to the preferred axis the vectors $\mathbf{M}_+$ and $\mathbf{M}_-$ bend toward $\mathbf{H}$, maintaining constant length until they coincide along $\mathbf{H}$, at which point the system becomes paramagnetic. The constancy of $|\mathbf{M}_+|$ and $|\mathbf{M}_-|$ is an exact property of the molecular field model, valid well below the Néel point.[34] For T close to T_N the projections of the sublattice magnetizations along the preferred axis are reduced according to the expression

$$|(\mathbf{M}_{\pm})_e| = M_0(T - \delta T_N). \tag{45}$$

This behavior is illustrated in Fig. 16(b).

B. Derivations

In this section we derive Eqs. (36), (37), (40), and (41) which form the basis for the discussion of the critical behavior in an applied field. In addition, the constancy of $|\mathbf{M}_+|$ and $|\mathbf{M}_-|$ under an applied perpendicular field for $T < T_N(\mathbf{H})$ will be proven.

In the molecular field model the microscopic interaction between the spins is replaced by an effective field. We assume that the spins of the (+) or (−) sublattices experience, in addition to the applied field $\mathbf{H}$, a field

$$\mathbf{H}_e^{\pm} = -\boldsymbol{\alpha}\cdot\mathbf{M}_{\mp} - \boldsymbol{\gamma}\cdot\mathbf{M}_{\pm}. \tag{46}$$

The tensor $\boldsymbol{\alpha}$ corresponds to the interactions between spins belonging to opposite sublattices while $\boldsymbol{\gamma}$ corresponds to the (somewhat weaker) interactions within a sublattice. Equation (46) is the same as Eq. (4.7) of Ref. 20, except that here we are putting the anisotropy directly into the molecular field equations through the use of tensor coupling constants. Equation (46) can be used to calculate the sublattice magnetizations for all combinations of temperature and field. For MnF_2, the correct behavior will, at least qualitatively, be obtained. For example, this formulation provides a description of

[34] This result was shown for the case $S = \frac{1}{2}$ in Ref. 19.

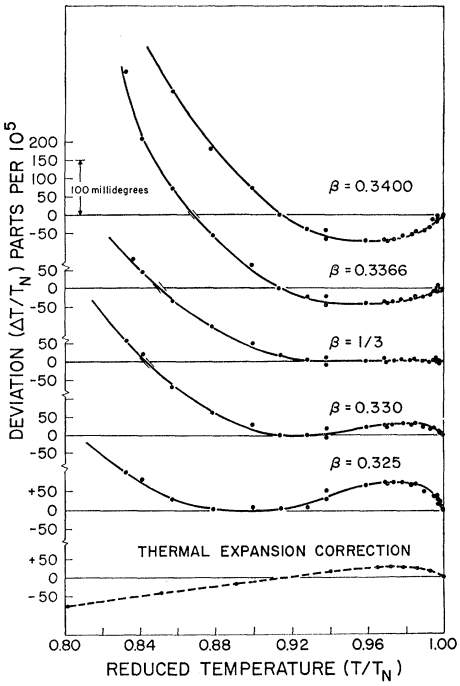

FIG. 13. Deviations from Eq. (34) for five choices of β. The most appropriate choice is the one for which the plot of $\Delta T/T_N$ versus T/T_N has no curvature as $T \to T_N$. The quantity ΔT is defined by Eq. (35). It represents the departure in temperature of a $\nu_0^{1/\beta}$ versus T plot from a straight line. The lowest curve represents the correction due to thermal expansion effects. This is discussed in Sec. 6.

the behavior of the susceptibility, including the slight anisotropy above T_N, the rise of the spontaneous magnetization below T_N, and the spin-flop phenomena observed below T_N in high fields. It is important to note that in writing (46) we are tacitly assuming that the contribution of the anisotropy to the molecular field is a linear function of the sublattice magnetizations. This would be a poor approximation if the anisotropy were due to a crystal field. For MnF_2, where the anisotropy is dipolar,[35] this approximation will be adequate. In fact, as will be discussed in II, this approximation leads to some important predictions[36,3] which are borne out experimentally. One of these concerns the behavior of the "staggered susceptibility" χ_s, a quantity figuring prominently in the analysis of the critical fluctuations. On this theory, the transverse components of χ_s do not diverge at T_N, behaving instead as $(T - T_1)^{-1}$ where T_1 is a temperature about 1.4°K lower than T_N. This result[36] has been substantiated by both the NMR linewidth[37] and neutron scattering data[38] near the critical point in MnF_2.

[35] F. Keffer, Phys. Rev. **87**, 608 (1952).
[36] T. Moriya, Progr. Theoret. Phys. (Kyoto) **28**, 371 (1962).
[37] P. Heller, in Proceedings of the Conference on Phenomena in the Vicinity of Critical Points, 1965 (National Bureau of Standards, Washington, D. C., to be published).
[38] K. C. Turberfield, A. Okazaki, and R. W. H. Stevenson, Proc. Phys. Soc. (London) **85**, 743 (1965).

For application to MnF_2, we assume that $\boldsymbol{\alpha}$ and $\boldsymbol{\gamma}$ have tetragonal symmetry about the preferred axis c. We denote the principal values in that direction by $\alpha_{\parallel}$ and $\gamma_{\parallel}$, respectively. We denote the principal values in the aa' plane by $\alpha_{\perp}$ and $\gamma_{\perp}$, respectively. We assume that $|\gamma_{\parallel}|<\alpha_{\parallel}$. Since isotropic interactions predominate over anisotropic interactions $\alpha_{\perp}/\alpha_{\parallel}\approx 1\approx\gamma_{\perp}/\gamma_{\parallel}$.

Suppose that for each sublattice there are N spins S per unit volume, each bearing a magnetic moment $Sg\mu_B$ where μ_B is the Bohr magneton and $g=2$. Then, in an applied field $\mathbf{H}$

$$M_{\pm}=M_{00}B_S[|\mathbf{H}-\boldsymbol{\alpha}\cdot\mathbf{M}_{\mp}-\boldsymbol{\gamma}\cdot\mathbf{M}_{\pm}|Sg\mu_B/(kT)], \quad (47)$$

where B_S is a Brillouin function and

$$M_{00}=NSg\mu_B=M_0(0)$$

is the saturated sublattice magnetization. In addition to Eq. (47) we must also require that $\mathbf{M}_{\pm}$ be collinear with $\mathbf{H}+\mathbf{H}_e^{\pm}$. Thus

$$\mathbf{M}_{\pm} \text{ is parallel to } \mathbf{H}-\boldsymbol{\alpha}\cdot\mathbf{M}_{\mp}-\boldsymbol{\gamma}\cdot\mathbf{M}_{\pm}. \quad (48)$$

Equations (47) and (48) completely define the predicted behavior with the additional stipulation that if several solutions exist, the physically correct solution has the least free energy.

It is convenient to throw Eqs. (47) and (48) into a symmetrical form in which the various physical quantities appear as dimensionless parameters. We define vectors

$$\mathbf{P}=\tfrac{1}{2}(\mathbf{M}_{+}+\mathbf{M}_{-})/M_{00}, \quad \mathbf{A}=\tfrac{1}{2}(\mathbf{M}_{+}-\mathbf{M}_{-})/M_{00},$$

which represent in reduced units the paramagnetic and antiferromagnetic parts of the magnetization, respectively. Next let

$$\theta=T/T_N,$$

where

$$T_N=(\alpha_{\parallel}-\gamma_{\parallel})Ng^2\mu_B^2S(S+1)/(6k).$$

(That this actually represents the Néel temperature will appear shortly.) The applied field is expressed by the dimensionless vector

$$\mathbf{F}=g\mu_B(S+1)(3kT_N)^{-1}\mathbf{H}.$$

A special function $G(x)$ is defined by writing

$$G(x)=B_S^{-1}(x)(S+1)/(3S)$$

which is essentially the inverse of a Brillouin function. This function depends on the spin S, but for simplicity we shall write simply $G(x)$ rather than $G_S(x)$. The behavior of $G(x)$ is indicated in Fig. 14. It may be shown that

$$G'(0)=1; \quad G'''(0)=-B_S'''(0)[B_S'(0)]^{-3}=(27/15)(2S^2+2S+1)/(S+1)^2; \quad G''(0)=0. \quad (49)$$

We define $G(\mathbf{V})$ where $\mathbf{V}$ is a vector by writing

$$G(\mathbf{V})=\mathbf{V}G(|\mathbf{V}|)/|\mathbf{V}|. \quad (50)$$

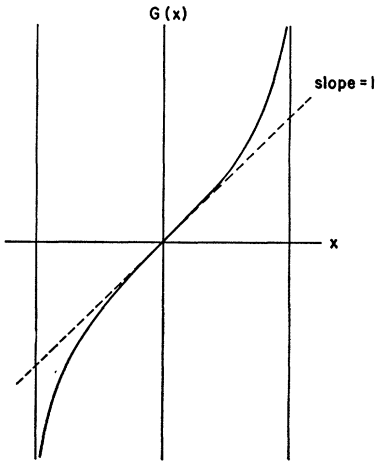

FIG. 14. The function $G(x)$.

The notation

$$\mathbf{V}_{\parallel}=(\mathbf{V}\cdot\mathbf{1}_c)\mathbf{1}_c, \quad \mathbf{V}_{\perp}=\mathbf{V}-\mathbf{V}_{\parallel} \quad (51)$$

will also be used to represent the parts of a vector $\mathbf{V}$ which are respectively parallel and perpendicular to the preferred axis.

With these conventions Eqs. (47) and (48) take the form

$$\tfrac{1}{2}[G(\mathbf{P}+\mathbf{A})-G(\mathbf{P}-\mathbf{A})]=(1/\theta)[\mathbf{A}_{\parallel}+Q\mathbf{A}_{\perp}], \quad (52)$$

$$\tfrac{1}{2}[G(\mathbf{P}+\mathbf{A})+G(\mathbf{P}-\mathbf{A})]=(1/\theta)[\mathbf{F}-W\mathbf{P}_{\parallel}-RW\mathbf{P}_{\perp}]. \quad (53)$$

Here, Q, R, and W are numerical factors given by

$$Q=(\alpha_{\perp}-\gamma_{\perp})/(\alpha_{\parallel}-\gamma_{\parallel}); \quad R=(\alpha_{\perp}-\gamma_{\perp})/(\alpha_{\parallel}+\gamma_{\parallel}); \quad W=(\alpha_{\parallel}+\gamma_{\parallel})/(\alpha_{\parallel}-\gamma_{\parallel}).$$

Note that $Q\approx 1\approx R$ since the anisotropy is slight. Also, W will be positive.

(i) *Zero-Field Solutions*

In zero applied field the system has no bulk magnetization and hence[39] $\mathbf{P}=0$. Then (52) yields

$$G(\mathbf{A})=(1/\theta)[\mathbf{A}_{\parallel}+Q\mathbf{A}_{\perp}]. \quad (54)$$

Since $G(\mathbf{A})$ is a vector parallel to $\mathbf{A}$, Eq. (54) has solutions for either $\mathbf{A}$ along or at right angles to the preferred axis. It is the first possibility which is of physical interest. In that case (54) becomes

$$G(A)=A/\theta. \quad (55)$$

Referring to Fig. 14, it can be seen that nontrivial solutions exist only for $\theta<1$. This corresponds to the fact that a spontaneous magnetization can exist only for $T<T_N$. Similar reasoning shows that a solution with $\mathbf{A}$ perpendicular to the preferred axis is mathematically

[39] This also can be shown formally from (53) with $F=0$, using the facts that $W>0$ and that $G(x)/x$ is a monotonically increasing function of x.

possible for $\theta/Q<1$, i.e., for $T<T_\perp$ where

$$T_\perp = QT_N. \tag{56}$$

Such a solution corresponds to an antiferromagnetic ordering along a transverse direction. We know experimentally that MnF_2 orders along the c axis. Evidently, then, the transverse solution is energetically less favorable, and so is unstable. This means that $Q<1$, i.e., that $T_\perp<T_N$. For MnF_2, where Keffer[35] has shown the anisotropy to be of dipolar origin, $T_N-T_\perp$ can be evaluated. This has been discussed elsewhere. The result[3,36]

$$T_N-T_\perp \approx 1.4°K \tag{57}$$

represents the anisotropy energy expressed as a temperature. Thus $Q=0.98$ for MnF_2.

The temperature dependence of the energetically favored solution in the critical region is now obtained by expanding $G(A)$ in a series

$$G(A)=A+\tfrac{1}{6}G'''(0)A^3+\cdots.$$

Since A is small near the Néel point, Eq. (55) leads to

$$A[1+\tfrac{1}{6}G'''(0)A^2]=A/\theta \tag{58}$$

or

$$A=[\tfrac{1}{6}\theta G'''(0)]^{-1/2}(1-\theta)^{1/2}.$$

Noting that the first term is slowly varying near the Néel point, we obtain Eq. (36) together with

$$D_N=[\tfrac{1}{6}G'''(0)]^{-1/2} \tag{59}$$

which, with (49), leads to Eq. (37).

(ii) *Effect of an Applied Field*

We now consider how the solution just obtained is altered by an applied field in the critical-temperature region.

At temperatures not too far below T_N ($A\ll 1$) and in moderate applied fields ($P\ll 1$), the left side of (53) is simply $\mathbf{P}$. We then find

$$\mathbf{P}_{II}=\mathbf{F}_{II}/(\theta+W), \quad \mathbf{P}_\perp=\mathbf{F}_\perp/(\theta+RW).$$

Since $R\approx 1$, this shows that $\mathbf{P}$ is proportional to and essentially colinear with $\mathbf{F}$ under the conditions of interest to us. This constitutes a verification of Eqs. (38) which we now write in the form

$$\mathbf{P}=\tfrac{1}{2}\chi_N\mathbf{H}/M_{00}. \tag{60}$$

Our procedure now is to regard $\mathbf{P}$ as a known quantity and feed it into Eq. (52) to calculate the temperature dependence of $\mathbf{A}$. The basic idea of this calculation is as follows: Let $G_P(\mathbf{A})$ denote the left-hand side of Eq. (52), i.e., let

$$G_P(\mathbf{A})=\tfrac{1}{2}[G(\mathbf{P}+\mathbf{A})-G(\mathbf{P}-\mathbf{A})]. \tag{61}$$

It may be seen that for small values of P and A, $G_P(\mathbf{A})$ considered as a function of $\mathbf{A}$ has the same general behavior as $G(\mathbf{A})$ except for an increased initial slope.

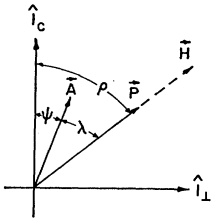

FIG. 15. Angles used in Sec. 5B(*ii*).

Equation (58) then becomes slightly modified. [See Eq. (65) below.] This results in a reduction of the Néel point, as will now be shown.

It is clear physically that the effect of the applied field is to rotate the sublattice magnetization vectors in the plane defined by the field and the preferred axis c. The vectors $\mathbf{P}$ and $\mathbf{A}$ are then coplanar with c, making angles ϕ and ψ with it, respectively. Since $\mathbf{P}$ and $\mathbf{H}$ are practically collinear, ϕ is essentially the angle between $\mathbf{H}$ and c as shown in Fig. 15. Also let $\lambda=\phi-\psi$, and let $\mathbf{1}_c$ and $\mathbf{1}_\perp$ denote unit vectors respectively parallel and perpendicular to c in the plane of the figure.

Expanding the right-hand side of (61) in a series we find

$$G_P(\mathbf{A})=\mathbf{A}\{1+\tfrac{1}{6}G'''(0)(A^2+P^2)\}+\mathbf{P}\tfrac{1}{3}G'''(0)\mathbf{P}\cdot\mathbf{A},$$

or equivalently,

$$\begin{aligned}G_P(\mathbf{A})=\mathbf{1}_c\{&A\cos\psi[1+\tfrac{1}{6}G'''(0)(A^2+P^2)]\\&+AP^2\cos\phi\cos\lambda\tfrac{1}{3}G'''(0)\}\\&+\mathbf{1}_\perp\{A\sin\psi[1+\tfrac{1}{6}G'''(0)(A^2+P^2)]\\&+AP^2\sin\phi\sin\lambda\tfrac{1}{3}G'''(0)\}.\end{aligned}$$

Writing $\phi=\lambda+\psi$ and performing some manipulations, the molecular-field equation (52) yields the pair of equations

$$\begin{aligned}A\{1+\tfrac{1}{6}G'''(0)[A^2+P^2(1+2\cos^2\lambda)]\}\\=(A/\theta)[1-(1-Q)\sin^2\psi],\end{aligned} \tag{62}$$

and

$$AP^2\cos(2\lambda)\tfrac{1}{6}G'''(0)=-(A/\theta)(1-Q)\sin\psi\cos\psi. \tag{63}$$

Suppose that the applied field is sufficiently weak so that

$$P^2\tfrac{1}{6}G'''(0)\ll 1-Q. \tag{64}$$

Then by (63), the vector $\mathbf{A}$ (if nonzero) will lie essentially along c, i.e., $\psi\approx 0$. In addition, (63) shows that in this case $(1-Q)\sin^2\psi$ will be negligible compared with $\frac{1}{6}P^2(1+2\cos^2\lambda)G'''(0)$. Also $\lambda\approx\phi$. Then Eq. (62) becomes

$$A[1+P^2(1+2\cos^2\phi)\tfrac{1}{6}G'''(0)+\tfrac{1}{6}G'''(0)A^2]=A/\theta. \tag{65}$$

On comparing this with (58), we see that the temperature dependence of A in the critical region is the same as in zero field with the exception of a downward shift in the Néel point. Using (59) and (60) we easily obtain Eqs. (40) and (41).

We must now consider how weak the applied field must be in practice in order to secure the condition

(64). Using (56), (59), and (60), (64) can be written

$$H^2(\tfrac{1}{2}\chi_N/M_{00})^2(T_N/D_N^2)\ll T_N-T_\perp,$$

which in light of (41) becomes essentially

$$|\delta T_N|\ll T_N-T_\perp. \tag{66}$$

In the NMR experiments $|\delta T_N|$ did not exceed 13 mdeg while $T_N-T_\perp\approx 1.4°$ so that this condition was always well satisfied. We should note, however, that our analysis was based on the assumption that the contribution of the anisotropy to the molecular field is proportional to the magnetization. If the anisotropy field were to decrease more rapidly than M as $T\to T_N$, we would have to regard $1-Q$ as temperature-dependent and decreasing. It is then conceivable that a behavior more complex than that predicted by (40) and (41) should take place in moderate fields. The simple behavior actually observed in the NMR experiments does not contradict this statement. This is because with the applied field either parallel or perpendicular to c, as was the case in the NMR experiments, the angle ψ will automatically be zero. Then Eqs. (40) and (41) should hold, until spin-flopping occurs, even in high fields.

(iii) *Effect of an Applied Field Perpendicular to the Preferred Axis*

In this case $\mathbf{M}_+$ and $\mathbf{M}_-$ bend toward $\mathbf{H}$ and have equal lengths M_0. Then Eq. (52) can be written

$$(1/M_0)(\mathbf{M}_+-\mathbf{M}_-)G(M_0/M_{00})=(\mathbf{M}_+-\mathbf{M}_-)/(\theta M_{00}),$$

or equivalently, assuming $\mathbf{M}_+-\mathbf{M}_-\neq 0$,

$$G(M_0/M_{00})=M_0/(\theta M_{00}).$$

This equation is independent of H. We conclude that as H is increased, the vectors $\mathbf{M}_+$ and $\mathbf{M}_-$ have constant length until they coincide along the direction of the field.

C. Comparison with Experiment

(i) *The Temperature Dependence of the Sublattice Magnetization*

A comparison between experiment and the molecular field theory results for $M_0(T)$ has already been given in Fig. 11. The magnetization rises much more rapidly than the theory predicts. In Table III we compare the reduced magnetization M_0/M_{00} obtained from the theory with the NMR results at a few temperatures just below T_N.

TABLE III. Reduced sublattice magnetization just below T_N.

T_N-T (mdeg)	M_0/M_{00} Experiment	M_0/M_{00} Molecular field theory, $S=\frac{5}{2}$
5	0.05	0.0125
20	0.08	0.025
100	0.137	0.056

TABLE IV. The field dependence of T_N.

Field orientation	K (mdeg/(10 kG)^2) Molec.-field theory	Experiment
c	−6.7	−19.5±3
a	−2.23	− 7.5±3

(ii) *The Field Dependence of T_N*

In Table IV we list the values of K in the expression $\delta T_N=-KH^2$ obtained from the experiments, together with the values computed from Eq. (41) using the numerical value for D_N given in Eq. (37) and the experimental susceptibility value given in Eq. (39).

The experimentally observed effects are about three times larger than the predicted ones. Note that the ratio of the Néel point shift for $\mathbf{H}$ along c to that for $\mathbf{H}$ along a is 3 to within experimental error. This ratio is thus consistent with Eq. (41).

The Néel point depression can be thought of as due to the effect of the external field in suppressing the antiferromagnetism. In interpreting the data it is instructive to examine the results of Tables III and IV together. At a given temperature below T_N the magnetization is *larger* than the theory predicts. On the other hand, the field required to bring the sample into the paramagnetic state is *weaker* than predicted. Hence the effect of a field in destroying a given spontaneous magnetization is considerably stronger than predicted.

For example consider the situation at 20 mdeg below T_N where $M_0/M_0(0)=0.08$. Application of a 10-kG field along the c axis lowers T_N by 20 mdeg, bringing the sample into the paramagnetic state. At this point Eq. (39) shows that the magnetization of either sublattice is $0.0085M_0(0)$. Hence the applied field has reduced the sublattice magnetization by about a factor of 10. We infer that in the process of increasing the field, the sublattice magnetizations behaved as sketched in Fig. 17(a). The corresponding behavior as deduced from Eqs. (40) and (41) is shown in Fig. 16(a).

Next consider the situation at 5 mdeg below T_N where $M_0/M_0(0)=0.05$. Application of an 8 kG field along the a axis lowers T_N by 5 mdeg bringing the sample into the paramagnetic state. Then by Eq. (39), $M_\pm=0.007M_0(0)$. Thus, the sublattice magnetization vectors have been greatly reduced in length as they bend toward the field. This is illustrated in Fig. 17(b). On the other hand, the molecular field model predicts a constant length as shown in Fig. 16(b).

(iii) *The "Law of Corresponding States"*

While the experiments are strongly at odds with the theoretical results in the form (40) and (41), they are in good accord with the theory in the form (42). This

has been shown in Sec. 4C, where we saw that the "law-of-corresponding-states model" discussed in Sec. 3 held. In terms of the sublattice magnetization vectors $\mathbf{M}_+$ and $\mathbf{M}_-$ the results of Sec. 3 can be written

$$\mathbf{M}_\pm(T,H)=\tfrac{1}{2}\chi\cdot\mathbf{H}\pm M_0(T-\delta T_N T/T_N)\mathbf{1}_c.$$

Since in the present experiments T/T_N was close to unity and δT_N was small this expression was for all practical purposes equivalent to Eq. (42).

6. THE EFFECTS OF THERMAL EXPANSION ON THE DATA

The dimensions of the MnF_2 lattice change slightly with temperature. This amounts primarily to a decrease in length along the c axis with decreasing temperature.[21] We can cite two mechanisms through which this shrinkage might affect the NMR data: (a) The alteration in the hyperfine coupling A; (b) The alteration in the exchange coupling J.

We first consider mechanism (a). The dependence of the hyperfine interaction on the lattice parameters can be estimated from the work of Benedek and Kushida.[11] They found

$$d\ln A/dP=1.9\times10^{-6}/\text{kg/cm}^2 \quad (67)$$

for the pressure dependence of the hyperfine interaction, and

$$d\ln c/dP=-0.31\times10^{-6}/\text{kg/cm}^2;$$
$$d\ln a/dP=-0.45\times10^{-6}/\text{kg/cm}^2, \quad (68)$$

for the pressure dependence of the lattice parameters. We infer that

$$d\ln A/d\ln c\approx-6. \quad (69)$$

To take account of this effect we will regard the saturated sublattice NMR frequency as a slightly temperature dependent quantity: instead of using Eq. (1) we will compute the reduced magnetization from the expression

$$M_0(T)/M_0(0)=\nu_0(T)/\tilde{\nu}_{00}(T)$$

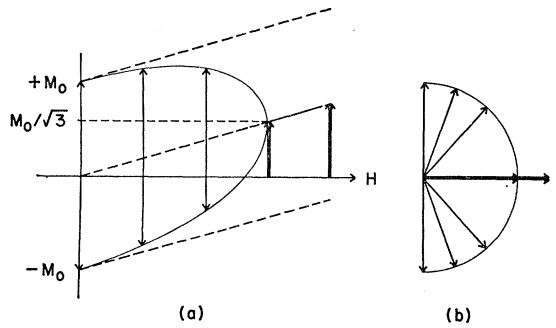

FIG. 16. Behavior of the sublattices with increasing field showing the transition to the paramagnetic state according to the molecular field theory. The vectors $\mathbf{M}_+$ and $\mathbf{M}_-$ are shown in the positions corresponding to five successively increasing values of the field, starting at $H=0$. (a) **H** along the preferred axis. (b) **H** perpendicular to the preferred axis.

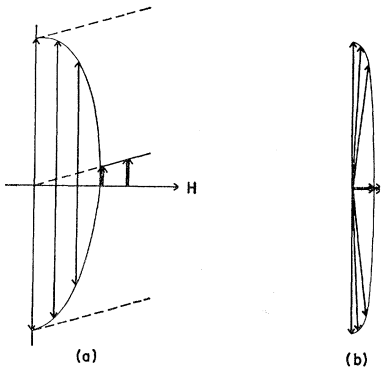

FIG. 17. Behavior of the sublattices with increasing field showing the transition to the paramagnetic state as deduced from experiment. The vectors $\mathbf{M}_+$ and $\mathbf{M}_-$ are shown in positions corresponding to five successively increasing values of the field, starting at $H=0$. (a) **H** along the preferred axis. (b) **H** perpendicular to the preferred axis.

where

$$\tilde{\nu}_{00}(T)=\nu_{00}\{1-6[c(T)-c(0)]/c(0)\}. \quad (70)$$

Accurate measurements of the thermal expansion have been reported by Gibbons.[21] Using his data in Eq. (70), $\tilde{\nu}_{00}(T)$ can be obtained. For $52°\text{K}<T<T_N$, the results can be expressed with sufficient accuracy by the empirical relation

$$\tilde{\nu}_{00}(T)=[159.15+0.02(T_N-T)(T_N-T+9°\text{K})\times(T_N-T+3°\text{K})^{-1}]\ \text{Mc/sec}. \quad (71)$$

We now consider mechanism (b). This effect does not alter the way in which the spontaneous magnetization is to be calculated from our data. However, it might affect a comparison of the data with a theoretical model in which J is constant. A theorist will ask: How would the sample have behaved if the manganese spins had been clamped in fixed positions? We will now provide an answer to his question.

The dependence of J on the lattice parameters is reflected in the results of Sec. 4A which may be written in the form

$$d\ln T_N/dP=4.4\times10^{-6}/\text{kg/cm}^2.$$

From (68) we estimate that the dependence of T_N on the lattice parameters is described by

$$d\ln T_N/d\ln c\approx-14. \quad (72)$$

We now regard the Néel point as a slightly temperature-dependent quantity given by

$$T_N(T)=T_N\{1-14[c(T)-c(T_N)]/c(T_N)\}. \quad (73)$$

In particular $T_N(T_N)=T_N=67.336°\text{K}$, while $T_N(T)$ increases as T falls below T_N on account of the contraction of the lattice.

For a mathematical magnetic system in which the Hamiltonian involves a single numerical parameter such as an exchange constant J, the magnetization will

depend in a certain way on the *reduced* temperature. Accordingly we suppose that our contracting sample behaves in the same way as a function of the effective reduced temperature $T/T_N(T)$. Thus in handing our results over to the theorist we should really plot the experimental data as a function of this quantity.

To take account of both effects (a) and (b) we should then plot the data in the form $\nu_0(T)/\tilde{\nu}_{00}(T)$ versus $T/T_N(T)$. In particular, in determining the constants D and β in the equation

$$M_0(T)/M_0(0)=D(1-T/T_N)^\beta \tag{74}$$

expressing the behavior of the clamped system, we should plot the data in the form

$$[\nu_0(T)/\tilde{\nu}_{00}(T)]^{1/\beta} \quad \text{versus} \quad T/T_N(T).$$

Then β is the value for which a straight line is obtained, and $-D^{1/\beta}$ is the slope of that line.

This procedure leads to the values $\beta=0.335$ and $D=1.193$. To demonstrate how the corrected data fit the power law (74) with these parameters, we define a quantity

$$\epsilon=1-T/T_N(T)-\{(1/D)[\nu_0(T)/\tilde{\nu}_{00}(T)]\}^{1/\beta},$$

which expresses the deviation from that law as a reduced temperature. On plotting ϵ versus $T/T_N(T)$ for several assumed values of β, a series of curves very much like those of Fig. 13 are obtained, the flattest curve corresponding to $\beta=0.335$. These new curves will be obtained from those of Fig. 13 by addition of the dotted correction curve shown at the bottom of that figure.

The dotted corrected curve was actually computed directly from Gibbons' data. The size of the circles corresponds to the resolution of his apparatus; their spacing corresponds to the roughly 0.5° spacing of his measurements in the critical region. It is clear that our conclusions would not have been very different had his measurements been more closely spaced. Of the two mechanisms (a) and (b) considered in computing the curve, mechanism (a) was relatively unimportant in affecting the exponent β, its effect being about one-fifth that of mechanism (b) and of the opposite sign.

The analysis just concluded has necessarily been simple. We have assumed that the magnetic Hamiltonian involves a single numerical parameter which depends just on the c-axis spacing. Nevertheless, from the small size of the estimated effects we can surely state that the critical behavior of the clamped system is described very accurately by a power law with indices

$$\beta=0.335\pm0.005 \quad \text{and} \quad D=1.193\pm0.01. \tag{75}$$

ACKNOWLEDGMENTS

The author is deeply grateful to Professor George Benedek for his thoughtfulness in suggesting this problem, for many valuable discussions during the course of the work, and for his comments on the manuscript. Thanks are also due to Professor T. Moriya for sending a copy of his paper prior to publication. We are greatly indebted to Dr. V. Jaccarino and Dr. H. Guggenheim of the Bell Telephone Laboratories for providing oriented single crystals of MnF_2. It is a pleasure to thank Dr. J. Jeener, Dr. Y. Obata, Dr. D. Gill, Dr. G. Seidel, Dr. T. Izuyama and Dr. K. Kawasaki for many helpful discussions.

APPENDIX A: CORRECTION FOR THE MISALIGNMENT OF THE SAMPLE

As explained in Sec. 2C, the applied field H_0 actually made a small angle $\delta\approx3.2°$ with the c axis for the measurements in which H_0 was nominally along c. We now compute how much the local field would be changed if perfect alignment were achieved. We first apply Eq. (11) to the case of imperfect alignment. Using the properties of the tensors p_α and p_β discussed in Sec. 3, we have

$$\mathbf{H}_{\text{nucl}}(\delta)=\pm\mathbf{1}_c H_I+\mathbf{1}_c(1+p_c)H_0\cos\delta+\mathbf{1}_\perp(1+p_\perp)H_0\sin\delta,$$

where the $(\pm)$ signs refer, respectively, to the α and β site resonances, $\mathbf{1}_\perp$ is a unit vector perpendicular to the c axis and $p_\perp$ is a number between 0.06 and 0.09. Then we compute that

$$H_{\text{nucl}}(0)-H_{\text{nucl}}(\delta)=\pm(H_0/H_{\text{nucl}})H_I(1+p_c)(1-\cos\delta)+\{(H_0^2/2H_{\text{nucl}})\sin^2\delta[(1+p_c)^2-(1+p_\perp)^2]\}.$$

The error thus introduced into the determination of p_c in the paramagnetic ($H_I=0$) is entirely negligible. For the antiferromagnetic state work the term in curly brackets was always less than 1 G and will be neglected. The misalignment correction then reads

$$H_{\text{nucl}}(0)-H_{\text{nucl}}(\delta)=\pm(H_0/H_{\text{nucl}})H_I(1+p_c)(1-\cos3.2°).$$

This correction was applied to all the data presented in Sec. 4.